Science of the Total Environment 920 (2024) 170800

Contents lists available at ScienceDirect

Science of the Total Environment

journal homepage: www.elsevier.com/locate/scitotenv

Review

Short-lived natural radionuclides as tracers in hydrogeological studies – A review

Michael Schubert [a,*], Mang Lin [b], Jordan F. Clark [c], Martin Kralik [d], Sandra Damatto [e], Lorenzo Copia [f], Stefan Terzer-Wassmuth [f], Astrid Harjung [f]

[a] Helmholtz Centre for Environmental Research GmbH – UFZ, Department Catchment Hydrology, Permoserstr. 15, 04318 Leipzig, Germany
[b] State Key Laboratory of Isotope Geochemistry and CAS Center for Excellence in Deep Earth Science, Guangzhou Institute of Geochemistry, Chinese Academy of Sciences, Guangzhou, 510640, China
[c] Department of Earth Science, University of California, Santa Barbara, CA 93106, USA
[d] Department Umweltgeowissenschaften, Division of Environmental Geosciences (EDGE) Center for Microbiology and Environmental Systems Science, University of Vienna, Josef-Holaubek-Platz 2, UZA II, Vienna A-1090, Austria
[e] Instituto de Pesquisas Energeticas e Nucleares (IPEN), Comissão Nacional de Energia Nuclear (CNEN), Av. Prof. Lineu Prestes, 2242 Cidade Universitaria, 05508-000 Sao Paulo, Brazil
[f] International Atomic Energy Agency, Department of Nuclear Sciences and Applications, Division of Physical and Chemical Sciences, Isotope Hydrology Section, Vienna International Centre, PO Box 100, 1400, Vienna, Austria

HIGHLIGHTS

- The presence of groundwater of sub-yearly residence time indicates high aquifer vulnerability.
- However, commonly used age tracers do not cover this short time range satisfactorily.
- A state-of-the-art review regarding the related use of ^{35}S, ^{7}Be, $^{32/33}P$, ^{222}Rn and $^{224/223}Ra$ is presented.
- Promising novel applications of these short-lived naturally occurring radionuclides are introduced.
- Examples of multi-tracer approaches employing the set of radionuclides are discussed.

GRAPHICAL ABSTRACT

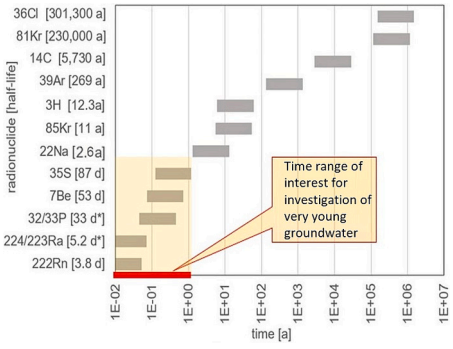

ARTICLE INFO

Editor: Christian Herrera

Keywords:
Tracer hydrology
Groundwater dating
Short-lived radiotracers
Multi-tracer approaches

ABSTRACT

Fundamental approaches to the study of groundwater rely on investigating the spatial and temporal distribution of stable and radioactive isotopes and other anthropogenic compounds in natural waterbodies. The most often used tracers for estimating groundwater flow paths and residence times, groundwater/surface water interaction as well as tracing chemical (contamination) sources include stable isotopes of water ($\delta\ ^{18}O$ and $\delta\ ^{2}H$), radiocarbon (^{14}C; $t_{1/2}$ = 5730 a), tritium (^{3}H; $t_{1/2}$ = 12.43 a) as well as unreactive fluorine-containing gases (e.g., chlorofluorocarbons CCl_3F or CFC-11; CCl_2F_3 or CFC-12; $C_2Cl_3F_3$ or CFC-113; and SF_6). While gas tracers are usually referred to as transient tracers and are appropriate for investigating modern flow systems, the isotopic tracers are often used to investigated paleo or regional flow systems. Stable isotopes of water can also be used to investigate groundwater/surface water interactions. Another, thus far been less frequently used group of

* Corresponding author.
E-mail address: michael.schubert@ufz.de (M. Schubert).

https://doi.org/10.1016/j.scitotenv.2024.170800
Received 15 December 2023; Received in revised form 15 January 2024; Accepted 6 February 2024
Available online 9 February 2024

groundwater tracers, are cosmo- and geo- genic short-lived radioisotopes. These isotopes are uniquely suited for studying a wide range of groundwater problems that have short time scales including high aquifer vulnerability to quantitative and qualitative impacts and groundwater discharge to surface waters. Here, we discuss and compare the applications of radio-sulphur (^{35}S; half-life $t_{1/2} = 87$ d), radio-beryllium (^{7}Be; $t_{1/2} = 53$ d), radio-phosphorus ($^{32/33}P$; combined $t_{1/2} = 33$ d), natural tritium (^{3}H; $t_{1/2} = 12.43$ a), radon (^{222}Rn; $t_{1/2} = 3.8$ d) and short-lived radium ($^{224/223}Ra$; combined $t_{1/2} = 5.2$ d). The paper discusses the principles of the individual tracer methods, focusing on the isotopes' input functions or values, on sampling techniques, and on methods of analyses. Case studies that applied a combined use of the tracers are referred to for readers who wish to learn more about the application of the so far underused cosmo- and geo- genic radioisotopes as aquatic tracers.

1. Introduction

Studies that focus on groundwater flow dynamics rely commonly on using (besides stable water isotopes) naturally occurring radionuclides as water residence time tracers (e.g., Kralik, 2015; Cook and Herczeg, 2000). For attaining robust results, the half-life ($t_{1/2}$) of the applied radionuclide needs to be in about the same range as the mean water residence time that can be expected for the investigated hydrological setting. Long-lived radionuclides, such as ^{3}H, ^{14}C, ^{36}Cl, ^{39}Ar, ^{81}Kr, and ^{85}Kr, are well-established as tools for dating of groundwaters older than ten years (Fig. 1) (e.g., Vogel et al., 1974; Loosli and Oeschger, 1979; Poreda et al., 1988; Ekwurzel et al., 1994; Sturchio et al., 2004; Corcho-Alvarado et al., 2013; Lindsey et al., 2019; Warr et al., 2023). In contrast, investigations that focus on very young groundwater are scarce (Fig. 1).

Reason for the lack of studies on very young groundwater is, that the vulnerability of groundwaters comes more and more into focus due to a worldwide increase in water scarcity triggered by land use change and an accelerated hydrological cycle (i.e., floods and droughts). Another reason is that straightforward analytical approaches and input functions for naturally occurring radionuclides, which show half-lives short enough to represent sub-yearly water residence times, have been developed only in the recent decades. Radon (^{222}Rn, $t_{1/2} = 3.8$ d) has widely been used as short-term tracer for investigating groundwater discharge into surface water bodies (Hofmann et al., 2011; Ortega et al., 2015; Adyasari et al., 2023). Short-lived radium nuclides (^{223}Ra, $t_{1/2} = 11$ d; ^{224}Ra, $t_{1/2} = 4$ d) and the ratio thereof (combined $^{224/223}t_{1/2} = 5.2$ d) have occasionally been used for the same purpose, however mostly in coastal settings (Hancock et al., 2006; Luek and Beck, 2014; Rodellas et al., 2017). Both radon and radium are of geogenic origin and naturally occurring in any aquifer mineral matrix (and hence in any groundwater). In recent years radionuclides of cosmogenic origin have been added to the short-term tracer portfolio for hydrogeological studies. The most promising candidates include ^{35}S ($t_{1/2} = 87.4$ d), ^{7}Be ($t_{1/2} = 53.3$ d) and $^{32/33}P$ (combined $^{32/33}t_{1/2} = 33$ d).

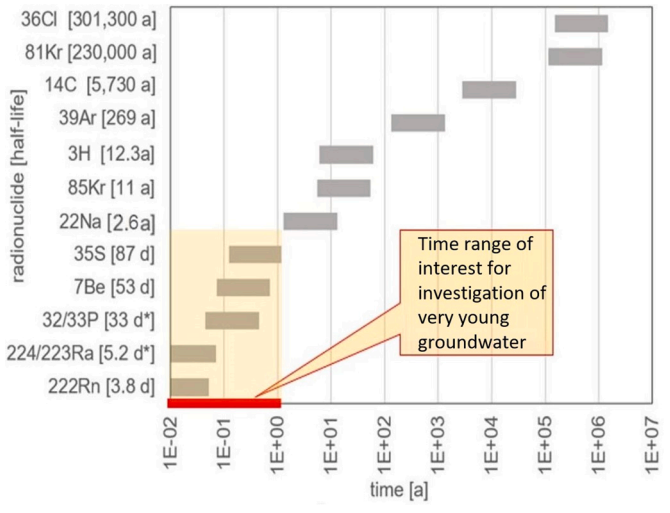

Fig. 1. Naturally occurring radionuclides suitable as water residence time tracers plotted versus approximately covered residence time ranges.

The two different origins of the addressed short-lived radionuclides, namely cosmogenic and geogenic, allow assigning them to three generally different tracer application concepts (Fig. 2). First, radionuclides of cosmogenic origin (i.e., ^{35}S, ^{7}Be and $^{32/33}P$) are continuously produced in the atmosphere. There they get dissolved in meteoric water or/and attached to aerosols and are conveyed by wet or/and dry deposition to the Earth's surface and finally to the groundwater. Within the subsurface their decay is not balanced by cosmogenic production anymore and their declining activity concentration indicates their (and thus the water's) residence time within the subsurface (Fig. 2 left).

Second, radionuclides of geogenic origin (i.e., ^{222}Rn and $^{224/223}Ra$) are generally absent in atmosphere and meteoric water. Their activity concentration in the water starts to build up from zero as soon as the water enters the subsurface. Since this increase is solely governed by the half-life of the nuclide and its aquifer-specific decay equilibrium (i.e., its groundwater endmember), the steadily increasing activity concentration is indicating the water residence time within the subsurface (Fig. 2 middle).

The third application concept does also apply to radionuclides of geogenic origin. If groundwater, which is in decay equilibrium with the aquifer, is discharged into a surface water body, the decay of the nuclide is not balanced by in situ production anymore. That results in a decline of its activity concentration, thus allowing the residence time of the freshly discharged groundwater to be assessed within the receiving surface water body based on a mass balance of the radionuclide within the surface water body (Fig. 2 right; see Fig. 8).

The presented review paper aims to summarize and evaluate short-lived cosmogenic (^{35}S, ^{7}Be, $^{32/33}P$, ^{3}H) and geogenic (^{222}Rn, $^{224/223}Ra$) radionuclides to be (jointly) applied as short-term residence time tracers. Aspects of sample collection, preparation, and measurement as well as data evaluation are discussed. Finally, future applications are outlined.

2. The tracer portfolio

2.1. Short-lived cosmogenic radionuclides (^{35}S, ^{7}Be, $^{32/33}P$)

2.1.1. Atmospheric radionuclide production and transport – general remarks

Any matter that is exposed to ionizing radiation undergoes changes in its isotopic properties. Although Earth is largely protected from cosmic radiation by its magnetic field ("cut-off rigidity"; see Section 2.1.5), part of the radiation (consisting of gamma-rays, electrons, single protons, alpha-particles as well as trace amounts of heavy ions and atomic nuclei) enters the Earth's atmosphere (Galvin et al., 1996; Feldman et al., 1998). Here the cosmic rays interact with terrestrial gas molecules resulting in nuclear transformations (through cosmic ray spallation or neutron capture). The gases that are mainly subject to cosmic ray spallation (and that are of relevance in the given context) are oxygen, nitrogen and argon.

The production rates of cosmogenic radionuclides within the

atmosphere are governed by the content of target nuclei at given atmospheric depth and kinetic energy of cosmic ray particles, and therefore vary with geographical latitude and atmospheric altitude. In general, production rates are higher in polar regions than equatorial regions, and peak at the upper troposphere and lower stratosphere (UTLS zone) (Lal and Peters, 1967). The varying solar activity has only minor impact because, averaged over time, the major fraction of the arriving cosmic radiation originates outside our solar system (e.g., Lal and Peters, 1967; Masarik and Beer, 1999; Poluianov et al., 2016).

The transport of the produced radionuclides from the UTLS zone down to the Earth's surface is strongly associated to the element-specific carrier medium and removal mechanism. ^{35}S and $^{32/33}P$ is conveyed mainly via wet deposition, i.e., dissolved as sulphate and phosphate, respectively (e.g., Tanaka and Turekian, 1991). In contrast, ^{7}Be is removed, attached to aerosols, by both dry deposition and physical scavenging by rain (e.g., Papastefanou and Ioannidou, 1995; Winkler et al., 1998). The difference in the physiochemical behaviours between ^{7}Be and ^{35}S has been used to constrain SO_2 deposition fluxes in the atmosphere (Turekian and Tanaka, 1992).

If a cosmogenic radionuclide is to be used as groundwater residence time tracer, its initial activity concentration needs to be considered. That requires setting up an input function covering the time previous to the actual groundwater study. The considered timespan depends on the half-life of the radionuclide. Any unsupported radionuclide inventory will have decayed by about 94 % after four half-lives. That means, e.g., in the case of ^{7}Be and ^{35}S that the input function should be based on data that covers six and twelve months, respectively. The required data is generally available for ^{7}Be (see "data evaluation" in Section 2.1.3; Terzi and Kalinowski, 2017; Zheng et al., 2021). In contrast, measurements of ^{35}S and $^{32/33}P$ in rain are very limited, which makes setting up their input functions challenging. The alternative application of proxy indicators, such as tritium (^{3}H) and ^{7}Be, is recently investigated (see Section 2.1.5 and Schubert et al., 2024).

Input functions of cosmogenic radionuclides are primarily shaped by (i) the annual cycle of large-scale air mass migration. This is overlain by (ii) non-cyclic medium-term stratosphere intrusion events, (iii) non-cyclic medium/short-term trends in both precipitation intensity and relative air humidity, (iv) non-cyclic anthropogenic activities and, to a minor degree, by (v) variations in the sun activity (generally following the eleven-years sun spot cycle). These cyclic and non-cyclic features are discussed in detail in the following paragraphs.

(i) The annual cycle of air mass migration

Conveying the produced activity inventories from the UTLS zone to the troposphere and finally down to the Earth's surface (and the groundwater) is tightly bound to the large-scale atmospheric cycles of stratosphere/troposphere exchange. The most relevant related process is the downward transport of air masses within the Hadley Ferrel Divergence Zone (HFDZ) located between two large-scale latitudinal atmospheric circulation cells, namely the Hadley Cell (in the equatorial region) and the Ferrel Cell (at midlatitudes) (Terzi et al., 2019) (Fig. 3).

The HFDZ changes its position in an annual cycle. In the northern hemisphere it is generally active at a latitude of about 30° (i.e., in northern Africa and northern Mexico). With the onset of the warm season it starts migrating north and approaches about 50° (i.e., central Europe and southern Canada). This results in latitudes of about 50° in distinct patterns with elevated activity concentrations in precipitation during the summer months. This pattern is intensified by a cyclic rise of the tropopause (Fig. 3) during the warm season. This upward shift increases the import of cosmogenic radionuclides from the UTLS zone to the lower atmosphere. Existing data on ^{7}Be, ^{35}S, ^{32}P and ^{33}P confirm this general temporal variance (Waser and Bacon, 1995; Delaygue et al., 2015; Schubert et al., 2020a; Terzi et al., 2020; Fig. 4).

(ii) Non-cyclic medium-term stratosphere intrusions

Stratosphere intrusions are large-scale dynamic processes that transport stratospheric air downward to the troposphere and even to the Earth's surface. The inference that activity concentrations of cosmogenic radionuclides in the atmosphere follow large-scale stratospheric intrusions into the troposphere was first reported by Lin et al. (2016, 2021) who reported related data for ^{35}S collected in western United States and the Himalayas, which are two global "hotspots" of deep stratospheric intrusion predicted by global climatology reanalysis data (Skerlak et al., 2014). Such deep stratospheric intrusion events enable significant amounts of cosmogenic radionuclides to reach the Earth's surface. In extreme episodes, ^{7}Be and ^{35}S activities in rain can be more than ten times above their annual averages (Lin et al., 2014; Lin et al., 2016). Monitoring these spikes, i.e., collecting data for setting up reliable input functions, requires the recording of adequate time series of ^{7}Be and ^{35}S in aerosols and precipitation, respectively.

If no such data is available, other meteorology and air quality parameters might be suitable as proxy parameters to indicate and quantify deep stratospheric intrusion events. For example, during such events high ozone (O_3) mixing ratios, low carbon monoxide (CO) mixing ratios, extremely low specific and relative humidity values as well as high

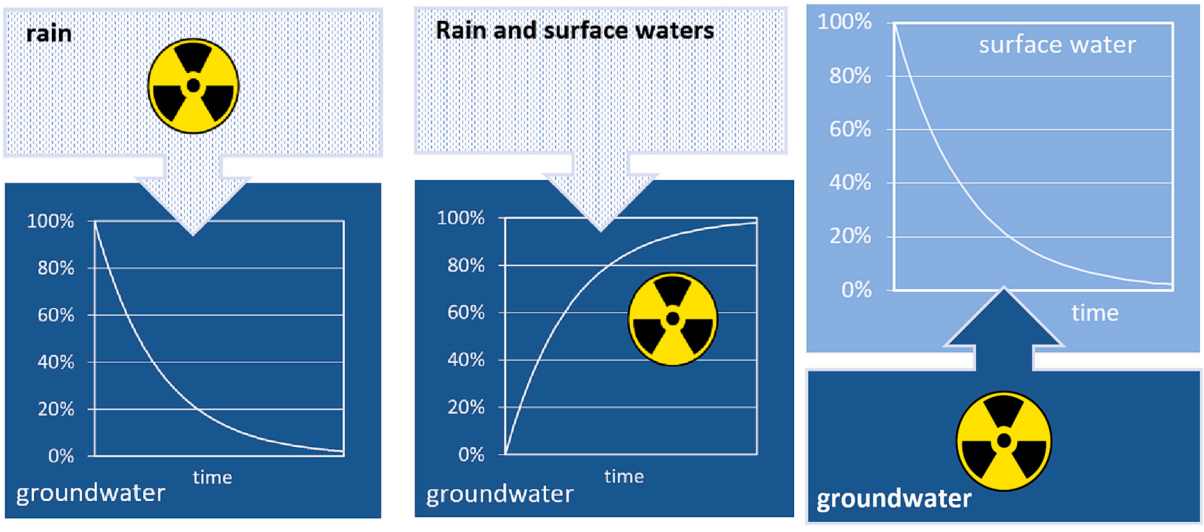

Fig. 2. The different origins of the radionuclides, namely cosmogenic (left) and geogenic (middle and right), results in different tracer application concepts. The x-axis is the decay time and y-axis the percentage of radionuclides relative to the respective steady state.

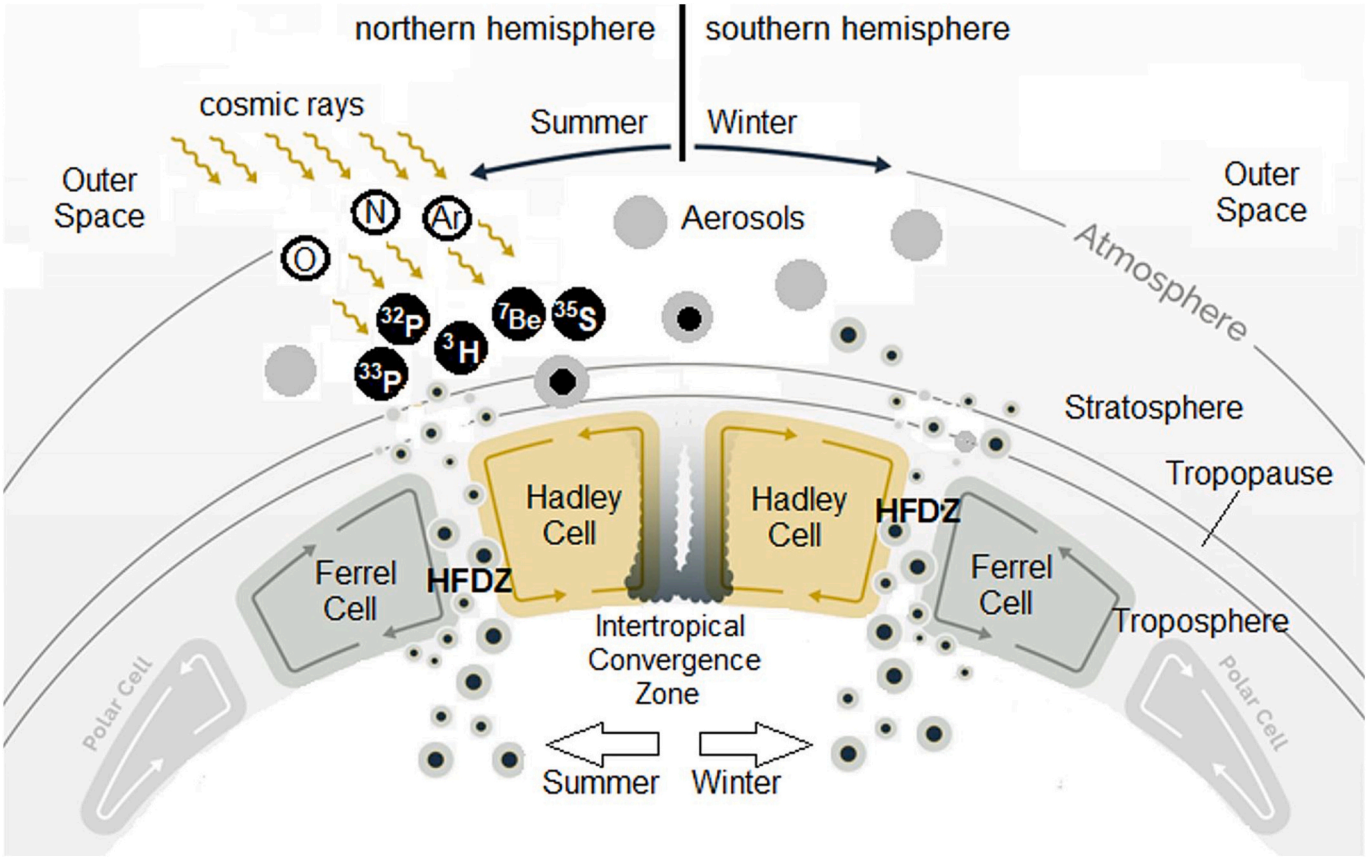

Fig. 3. Schematic image illustrating ^{7}Be and ^{35}S production within the stratosphere by cosmic ray spallation and their conveying toward the earth's surface via the HFDZ that is shifting in place with the seasons as indicated by the arrows (Schubert et al., 2020a, 2020b, 2020c, 2020d).

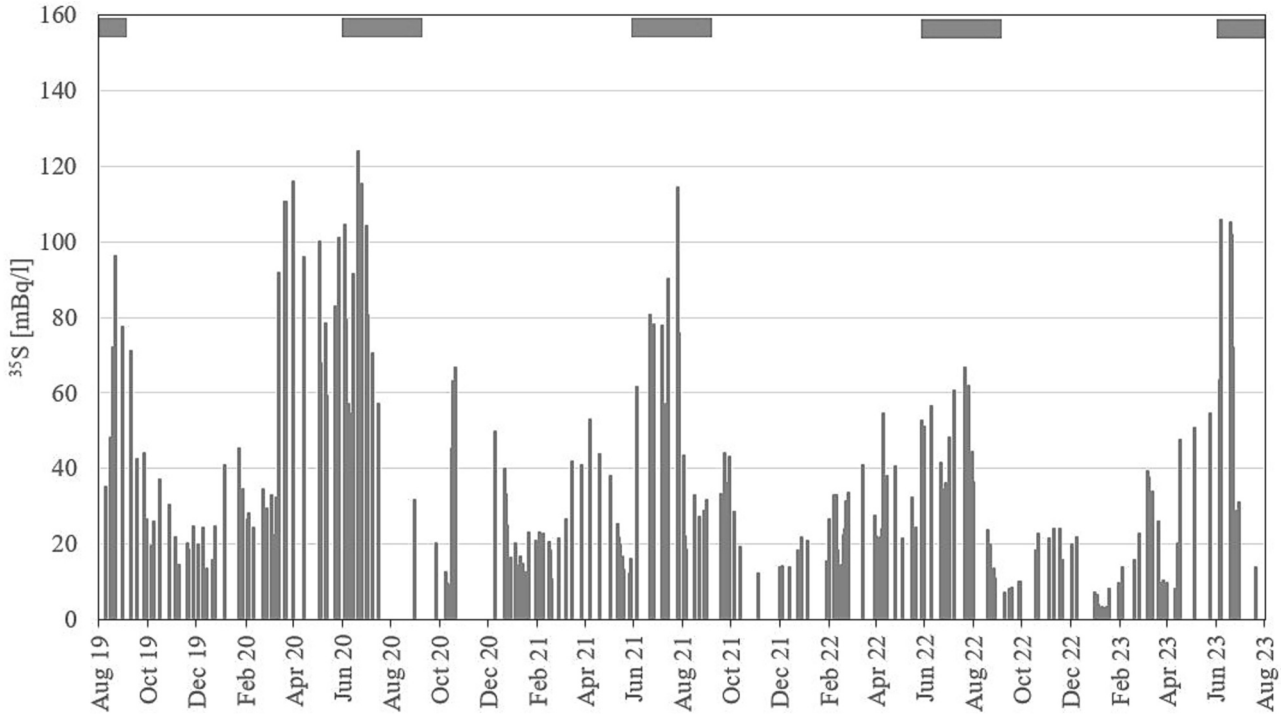

Fig. 4. ^{35}S in rain recorded close to Leipzig, Germany (Schubert pers. comm., 2023); moving average over three consecutive events; the bars indicate the summer months June–August.

values of potential vorticity are usually simultaneously observed (Cristofanelli et al., 2010; Lin et al., 2016). More comprehensive meteorological modelling approaches that include these parameters would allow delineating the impact of deep stratospheric intrusion events more precisely (Lin et al., 2016). Though, we note that these indicators have their own limitations. For example, there are multiple sources for O_3. High O_3 mixing ratios could originate from both the stratosphere and in situ photochemical formation at the Earth's surface. Hence, cosmogenic radionuclides remain the most sensitive and unambiguous tool for monitoring stratospheric intrusion events.

2.1.1.1. Transport by non-cyclic medium/short-term precipitation and humidity patterns. Periods of enhanced wet deposition, triggered by long-lasting (several days) precipitation events but also by periods of high relative air humidity, result in a temporary decrease of the atmospheric content of cosmogenic radionuclides. Washout of radionuclides during single rain events and was reported both for ^{7}Be (Kusmierczyk-Michulec et al., 2015) as well as ^{35}S (Schubert et al., 2020a, 2020b, 2020c, 2020d). To estimate the impact qualitatively, it can be described analogue to an exponential decay (e.g., McMahon and Denison, 1979). Comparable to the decay constant, a "scavenging coefficient" (unit: 1/day) is used to calculate a "0.5-folding time", which determines how much time it takes wet deposition to decrease the element-specific activity concentration to half of its initial value (Kusmierczyk-Michulec et al., 2015).

However, such medium-term activity fluctuations due to washout by precipitation are of only minor relevance for the use of cosmogenic radionuclides as short-term water residence time tracers. The half-lives of the applicable radionuclides are long enough to level out these short-term fluctuations in the ground- and surface water bodies.

In contrast, extreme rain events are generally associated to intense surface water runoff, i.e., rainwater that does not reach the aquifer but is directly discharged into the local receiving surface water body. That results in lower fluxes of meteoric water and hence of short-lived cosmogenic radionuclides to the groundwater, potentially indicating too long residence times.

2.1.1.2. Impact of non-cyclic anthropogenic activities. For the short-lived radionuclides in focus here, the impact of the late 1950s and early 1960s thermonuclear bomb tests have vanished. Still, such anthropogenic influence remains possible. For example, the Fukushima nuclear power plant was damaged by the March 2011 earthquake and a concomitant tsunami. At the beginning of this disaster several hundred tons of seawater were used to cool a partially melted reactor core. The chlorine (^{35}Cl, stable) dissolved in the seawater captured neutrons emitted from the reactor core thereby producing significant amounts of ^{35}S via an (n, p) reaction in which a neutron enters a nucleus and a proton leaves the nucleus simultaneously. At a site near the power plant, atmospheric ^{35}S activities were detected to be about 100 times greater than usual (Priyadarshi et al., 2013). This impact was even detected at the far side of the Pacific Ocean (Priyadarshi et al., 2011). Although such events are extremely rare, anthropogenic activities may complicate the interpretation of short-lived natural radionuclide data (e.g., Schubert et al., 2020a, 2020b, 2020c, 2020d).

2.1.1.3. Impact of cyclic long-term variations of the sun activity. As mentioned above, only a minor fraction of the cosmic radiation that reaches the UTLS zone originates in the Sun's corona. Still, it has to be considered (e.g., Lal and Peters, 1967; Masarik and Beer, 1999; Poluianov et al., 2016). Short-term events of extreme solar activity, such as solar proton storms, can significantly increase cosmogenic radionuclide production temporarily (though such solar storms, also called "hard events", have been rare in the recent past; Mekhaldi et al., 2021). During a long-term solar maximum, the strong solar wind shields the Earth from high-energy cosmic rays and reduced thus the flux of cosmic particles that reach the UTLS zone. Hence, the production rate (and measured activity) of short-lived cosmic radionuclides is lower during solar maxima within the regular 11-year solar cycle. Lin and Thiemens (2022) found that ^{35}S activities at solar maximum are only ~44 % of those at solar minimum. The production rate of ^{7}Be was reported to vary about 20 % from its mean depending on the solar stage (e.g., Koch et al., 1996; Koch and Rind, 1998). The impact of the long-term solar cycle on cosmogenic radionuclide production rates including ^{7}Be could be reasonably predicted via rigorous determinations of production yield functions that describe radionuclide productions by cosmic rays (with known kinetic energy) at given altitude and latitude and cross-sections of corresponding nuclear reactions between target nuclei in the atmosphere and primary/secondary particles from cosmic rays (Poluianov et al., 2016), but related works that focus on ^{35}S and $^{32/33}$P production remain lacking and should be carried out.

Resulting from the aforesaid, the natural cosmogenic radionuclide activity concentration in rain in a certain region depends on the production rate in the UTLS, the intensity of long-term and short-term stratosphere/troposphere exchange, the varying intensity of wet scavenging, and also on the horizontal transfer of air masses from neighbouring latitudes. Local short-term climate patterns and seasonally changing atmospheric transport processes are additional factors that govern the deposition rate. Some ranges of natural cosmogenic radionuclide activity concentration in rain shall be given here. The annually varying ^{35}S activity in rain ranges between ~5 and ~ 150 mBq/l (e.g., Osaki et al., 1999; Hong and Kim, 2005; Cho et al., 2011; Urióstegui et al., 2015; Schubert et al., 2020a, 2020b, 2020c, 2020d). ^{32}P and ^{33}P timeseries ($n = 30$) recorded at Bermuda Island (ca. 31°50′N) covering a period of 12 months (Waser and Bacon, 1995) showed activity concentrations between about 2.5–23.5 mBq/l for both isotopes. The timeseries indicated elevated values between July and September. However, the annual $^{32/33}$P pattern was by far not as pronounced as the one presented by Schubert et al. (2020a) for ^{35}S. The reason is that the ^{35}S samples were collected far more north and hence more impacted by the HFDZ latitudinal shift. Present-day levels of ^{3}H in precipitation vary about 100–3000 mBq/l (Morgenstern and Taylor, 2009; Palcsu et al., 2018; Terzer-Wassmuth et al., 2022a, 2022b). ^{7}Be measured in precipitation over five years in Sao Paulo, Brazil, varied between 1000 and 6000 mBq/l (Damatto pers. comm., 2023) and up to 10,000 mBq/l in precipitation in Thessaloniki, Greece (Ioannidou and Papastefanou, 2006).

2.1.2. Radio-sulphur (^{35}S)

2.1.2.1. Natural occurrence and properties of radio-sulphur. ^{35}S is produced in the upper atmosphere by cosmic ray spallation reaction with ^{40}Ar. Its half-life is 87.4 days (beta decay; maximum decay energy: 167 keV; decay product: ^{35}Cl). ^{35}S rapidly oxidizes to SO (lifetime <1 ms) and then SO_2 (in ~1 s) (Black et al., 1982; Brothers et al., 2010) and eventually to SO_4^{2-}. $^{35}SO_4^{2-}$ gets dissolved in meteoric water, i.e., it enters the water cycle in the troposphere.

Sulphate (and hence $^{35}SO_4^{2-}$) is highly mobile in groundwater, i.e., is not retarded by any mineral matrix. Furthermore, it displays chemical stability over a wide range of hydrochemical conditions. Under slightly reducing and oxic conditions sulphate is transported with the groundwater conservatively (Knöller et al., 2005). Still, under stronger reducing conditions, it may be subject to bacterial sulphate reduction if a bioavailable electron donor (e.g., DOC) is present (Lovley and Chapelle, 1995; Knöller et al., 2008, Knöller and Schubert, 2010; Guo et al., 2021). In this case, the application of ^{35}S as residence time tracer is limited because the fractionation factors required for correcting the ^{35}S analytical results for sulphate degradation have not been investigated to date. However, bacterial sulphate reduction predominantly affects deep aquifer systems, which are not targeted by short-term residence time tracers. If stable (sulphate) reducing conditions are met in a shallow

aquifer, as it may occur in wetlands or floodplains, they indicate very limited exchange with meteoric water and hence groundwater residence times that are also out of the age range covered by short-term tracers such as ^{35}S. Bacterial sulphate reduction might also occur in localized aquifers portions below landfills (Christensen et al., 2001).

2.1.2.2. Application concept for using radio-sulphur as aqueous tracer. Whereas ^{35}S activities in rain are continuously supported by cosmic ray spallation, there are no natural ^{35}S sources in the subsurface. Related traces from experiments using radio-labelled compounds to understand sulphur biogeochemistry (e.g., Grunbaum et al., 1990; Wang et al., 2023) are negligible in most cases. This allows using ^{35}S as indicator for the time that has elapsed since the meteoric water was isolated from atmospheric ^{35}S production, i.e., since it entered the subsurface.

However, due to the varying ^{35}S activity in precipitation (Fig. 4), using a discrete initial value is not appropriate. A ^{35}S input function is required for sound evaluation of the ^{35}S data. Due to the ^{35}S half-life, this input function should preferably cover a period of twelve months (~4 $t_{1/2}$) but at least of six months (~2 $t_{1/2}$) prior to the groundwater sampling campaign. That requires either a systematic long-term investigation of ^{35}S in rain in the study region or/and the recording of more easily attainable proxy values (Schubert et al., 2020a, 2020b, 2020c, 2020d, 2023). Hence, if groundwater dating is to be executed based on ^{35}S, it is recommended to collect and analyse at least a few rain samples in the months prior to the actual sampling campaign for their ^{35}S activity concentration in order to set up a ^{35}S input function. This should be done considering the general annual pattern of higher ^{35}S activities in summer and lower ^{35}S activities in winter. As a rough estimate, Schubert et al. (2020a, 2020b, 2020c, 2020d, 2023) suggest that the ^{35}S activity concentrations during summer are on average about three times as high as during winter.

Based on this tracer application concept, ^{35}S has been used to determine travel times of sulphate in watersheds (Cooper et al., 1991; Michel et al., 2000, 2002), to estimate the fraction of recent snowmelt in base flow (Cooper et al., 1991; Urióstegui et al., 2017), to determine groundwater residence times near managed aquifer recharge facilities (Clark et al., 2016; Urióstegui et al., 2016), and to evaluate the vulnerability of aquifers (Kralik et al., 2016) (see Section 3).

2.1.2.3. Sampling, sample preparation and measurement of radio-sulphur in water samples. Groundwater and surface water can be sampled without specific precautions. Rain samples should be collected in a way that allows a sample volume of at least 10 l per rain event. If collection of weekly or monthly composite samples is intended, the volume of the container should be chosen in accordance to the expected cumulative precipitation amount. In the case of monthly composite rain samples the decay of ^{35}S during the time of collection has to be considered. If containers with a wide opening are used, noteworthy evaporation of the sample and dry deposition may occur during the time of collection.

Measurement of ^{35}S in water samples is executed by means of a liquid scintillation counter (LSC). To allow statistical reliability of the detection results a sufficient ^{35}S activity is mandatory. The required water sample volume depends therefore on (i) the detection limit of the LSC in use and (ii) the activity inventory of the sample. Experience shows that for both rain and groundwater a water sample volume of 20 l is generally sufficient to meet the requirements (Schubert et al., 2019, 2020d).

Essentially, sample preparation aims on quantitatively extracting the dissolved sulphate from the water sample and concentrating it to a volume that fits (together with the required amount of scintillation cocktail) into an LSC vial (20 ml). Since handling of 20 l samples both in the field and in the laboratory is cumbersome, on-site sulphate extraction from the sample is possible, e.g., by pumping the water through a cartridge filled with an ion exchange resin (Deinhart et al., 2021).

Applicable scintillation cocktails, namely Hionic-Fluor® and Insta-Gel Plus® (both PerkinElmer) accept only certain sulphate loads. The water-soluble scintillation cocktail Hionic-Fluor® (18 ml) accepts sulphate loads of up to 100 mg, which equals a maximum sulphate concentration of 5 mg/l in 20 l of water (Schubert et al., 2020a, 2020b, 2020c, 2020d). Hence, it is suitable for rain water samples. Groundwater is generally higher in sulphate, which entails the use of the scintillation cocktail Insta-Gel Plus®. The two different sample preparation approaches are briefly summarized in the following. The sample preparation methods are described more detailed in the cited literature.

For water samples low in total sulphate a batch method is used for sulphate extraction (Schubert et al., 2020d). Two gram of the weak-base exchange resin Amberlite IRA67 (which are first prepared with acetic acid) are added to the 20-litre water sample and stirred for several hours (ideally overnight), e.g., by means of a magnetic stirrer. Subsequently, the sulphate is eluted off the resin with ammonium hydroxide. The high ionic strength of the resulting eluent solution is substantially reduced by evaporating the eluate to dryness (under a fume-hood). The resulting water-soluble precipitate ($[NH_4]_2SO_4$) is dissolved in 2 ml deionized tritium-free H_2O resulting in a pH neutral solution of an ionic strength that is acceptable for Hionic-Fluor®. 10 ml of the cocktail are added. After shaking the vial can be measured by LSC. A comparable ion exchange approach reported by Lin et al. (2017) uses the resin AG1-X8.

In case of samples with high ionic strength, the scintillation cocktail Hionic-Fluor® is not suitable. After extraction with Amberlite IRA67 and re-elution (as above), sulphate is therefore quantitatively precipitated from the sample as $BaSO_4$ by adding aqueous $BaCl_2$ solution (Urióstegui et al., 2015). Afterwards, the supernatant water is decanted and the $BaSO_4$ precipitate is transferred into an LSC vial. Subsequently Insta-Gel Plus® is added to the vial and the vial is shaken until complete gelation and apparent homogeneity.

Groundwater and surface water samples might require additional sample preparation steps that aim at "cleaning" the sample to minimize physical and colour quench during LSC measurement. These steps include (multiple) decantation of the 20-litre sample, filtration, or treatment of the sample or the precipitate with H_2O_2 (Lin et al., 2017; Lin and Thiemens, 2018) to get rid of potentially present organic material. No standardized preparation protocol can be suggested here as the steps depend on the individual sample.

The same holds for the optimum settings of the LSC (e.g., assay type, quench indicator, counting energy window, coincidence time) as they depend on the counter in use. Exemplary settings for TriCarb 3170 Tr/SL and Quantullus GCT 6220 have been suggested by Schubert et al. (2020a, 2020b), respectively.

2.1.2.4. Data evaluation. To obtain ^{35}S activity at the time of sampling, the time that has elapsed between sampling and measurement needs to be considered. The apparent age of a groundwater sample (t) is determined based on its ^{35}S activity concentration (C_t) and the site-specific initial ^{35}S value (C_0) applying the general decay equation, with λ being the decay constant ($\lambda = \ln 2/t_{1/2}$) for ^{35}S, namely 9.17 * 10^{-8} s^{-1} (Eq. (1)).

$$C_t = C_0 \times e^{-\lambda t} \quad (1)$$

The initial ^{35}S value (C_0) has to be derived from the regional ^{35}S input function. The input function has to be carefully set up based on a reasonable number of previously recorded ^{35}S-in-rain values covering at least six months prior to the groundwater sampling campaign. Generally, monthly integrated samples are adequate for the purpose. If only an inadequate number of ^{35}S-in-rain values is available, proxy parameters set in context to the generally known pattern of cosmogenic radionuclides (see Section 2.1.1) can help to set up an adequate input function (for proxy values ^{7}Be and ^{3}H see Sections 2.1.3 and 2.1.5, respectively).

2.1.3. Radio-beryllium (^{7}Be)

2.1.3.1. Natural occurrence and properties of radio-beryllium.

Radio-beryllium (^{7}Be) is produced through cosmic ray spallation of atmospheric oxygen, nitrogen and carbon primarily within the UTLS zone (Lal and Peters, 1967; Koch and Rind, 1998; Tilley et al., 2002). It decays by β decay (with γ emission at 477.61 keV; Firestone et al., 1996) with a half-live of 53.2 days. The decay product is ^{7}Li.

The maximum ^{7}Be production occurs in about 20–30 km atmospheric altitude (Usoskin and Kovaltsov, 2008), resulting in about 75 % of the UTLS-born ^{7}Be being produced in the lower stratosphere and about 25 % in the upper troposphere. The average production rate of ^{7}Be in UTLS zone is estimated to be 810 atoms m^{-2} s^{-1}; its mean activity concentration in the troposphere is about 12.5 Bq m^{-3} (Ioannidou and Papastefanou, 2006). Atmospheric ^{7}Be production at sea level is about two to three orders of magnitude lower than in the stratosphere (Usoskin and Kovaltsov, 2008). The ^{7}Be production rate also varies temporarily in given elevations (e.g., Koch and Rind, 1998; Pham et al., 2011).

Within its primary production zone (ULTS) ^{7}Be attaches quickly to submicron size aerosol particles (e.g., Lange, 1994; Ioannidou and Papastefanou, 2006), which are subsequently conveyed down to Earth by intrusion of stratospheric air masses into the troposphere followed by both wet and dry deposition (Kusmierczyk-Michulec et al., 2015; Terzi and Kalinowski, 2017). Several studies revealed that wet deposition, i.e., washout by precipitation, is substantially more effective than removal by dry deposition (e.g., McNeary and Baskaran, 2003). A comprehensive data collection on global ^{7}Be data was published by Zhang et al. (2021). The authors summarize that the fraction of dry deposition of ^{7}Be is highly variable, ranging from 1 % to 44 % but being in general around 12 ± 9 % of its total deposition. The data compilation reveals furthermore distinct latitudinal variabilities of both atmospheric ^{7}Be concentration and deposition, generally with concentrations and fluxes highest at the mid-latitudes and decreasing toward the Equator and poles (see also Lal and Peters, 1967). The data suggests concentrations and fluxes ranging globally between 0.33 and 17.77 mBq m^{-3} and 59–6350 Bq m^{-2} yr^{-1}, respectively.

2.1.3.2. Application concept for using radio-beryllium as aqueous tracer.- ^{7}Be is established as tracer for monitoring and studying large-scale atmospheric processes and validating global atmosphere circulation models (Hernández-Ceballos et al., 2015). Within this field of application ^{7}Be is frequently used for studying cloud build-up and precipitation formation, mainly on a local scale (e.g., Koch et al., 1996; Ioannidou and Papastefanou, 2006; Hedfords et al., 2010; Pham et al., 2011; Doering and Saey, 2013) as well as for investigating transport and residence time of aerosols in the atmosphere (e.g., Kaste et al., 2002). Furthermore, ^{7}Be deposition is used as indicator for detecting and tracing nuclear accidents as well as for soil erosion studies and studies on reservoir sedimentation. However, these applications are out-of-scope of this review and the reader is referred to related comprehensive publications, e.g., IAEA (2014) or Taylor et al. (2019).

Related to the subject discussed here, ^{7}Be can in principle be used as indicator for the presence of very young groundwater. Due to its short half-life and the absence of natural or anthropogenic ^{7}Be sources in the subsurface, the ^{7}Be activity of any meteoric water will decline to about 6 % after 213 days (four half-lives).

However, regarding hydrogeological studies, the use of ^{7}Be is limited due to its strong tendency to get adsorbed to soil particles in the upper soil layers (Hohwieler, 2005; Iurian et al., 2013). Hohwieler (2005) reported a retention of 90 % of ^{7}Be in the soil layer through column experiments. Frey et al. (2011) were able to measure ^{7}Be in surface water and groundwater deducing residence time estimates that were consistent with other tracers. They used the retention reported by Hohwieler (2005) but recommended column or lysimeter experiments with the soil collected from the individual recharge area.

The mobility of ^{7}Be in the subsurface is decreasing with increasing pH of the percolating water but increasing with the presence of free fluoride and dissolved organic carbon (Veselý et al., 1989). ^{7}Be activity concentrations in surface waters and groundwaters are therefore dependent on pH, presence of fulvic acids and suspended sediments (Kaste et al., 2002). While the input function for ^{7}Be is relatively easy to obtain due to extensive research on atmospheric behaviour and cycling (incl. data collected by IMS network of monitoring stations; see below), its tracer application to surface and groundwater needs further research and might be limited to very specific study cases (e.g., shallow karst aquifers without soil covers).

2.1.3.3. Sampling, sample preparation and measurement of radio-beryllium in water samples. For the collection of wet ^{7}Be deposition polyethylene rain collectors are generally used. They are installed at least 1 m above the ground to avoid soil particles in the sample. To obtain a sufficient sample volume for the ^{7}Be measurement (i.e., a countable activity), the rain is usually collected as composite sample on a weekly or monthly basis, depending on the frequency and intensity of rain events. Prior to exposure, a small volume of diluted HNO_3 or HCl is added to the collection container in order to prevent beryllium adsorption onto the container walls (Vallés et al., 2009; Taylor et al., 2016; Courtier et al., 2017; Mohan et al., 2018).

Gamma-ray detection is used for measuring ^{7}Be. After collection, the water samples are filtered using paper filters (e.g., Whatman, grade 41 or 42) and subsequently evaporated to reduce the total sample volume to fit the applied gamma-ray detection geometry (Taylor et al., 2016; Mohan et al., 2019). Some authors prefer to co-precipitate ^{7}Be with iron hydroxide (Courtier et al., 2017) or potassium permanganate (Taylor et al., 2016) aiming to increase the sensitivity of the gamma-ray measurement.

Even though it is out of the direct scope of this paper, it shall be mentioned that atmospheric ^{7}Be is routinely sampled and measured at CTBTO stations worldwide as dry deposition with high-volume aerosol samplers (see "data evaluation" section below). The typical CTBTO sampling approach relies on continuously filtering air at a rate of 500–1000 m^3/h with samples being collected on a daily basis. The approach allows catching over 80 % of the air-bound particles larger than 0.2 μm. The continuous time series of ^{7}Be data collected on a daily basis allow using the recorded datasets as proxy for other short-lived cosmogenic radionuclides such as ^{35}S, which makes it interesting in the given context (see "data evaluation" section below).

The ^{7}Be activity concentration in both aerosol and water samples is measured with high-resolution germanium detectors (Courtier et al., 2017; Mohan et al., 2019; Schulze et al., 2000; Medici, 2001; Morera-Gómez et al., 2022). The minimum detectable activity concentration depends on the applied detection system but is on average about 5–30 μBq/m^3 for filtered aerosol (Kusmierczyk-Michulec et al., 2015) and about 0.15–0.5 Bq/l for water (Damatto pers. comm., 2023).

2.1.3.4. Data evaluation. Due to the tendency of beryllium to get adsorbed onto the soil and aquifer matrix, quantitative evaluation of ^{7}Be activities in groundwater is challenging. Still, the presence of ^{7}Be in groundwater confirms the presence of very young groundwater in the aquifer and is therefore qualitatively indicating a high aquifer vulnerability.

Besides being used as qualitative aquifer vulnerability indicator, ^{7}Be activity concentrations in aerosol samples recorded as long-term time series can be used as proxy parameter for setting up a ^{35}S input function. Since ^{35}S and ^{7}Be are produced by the same process in the same atmospheric altitude, the ^{7}Be time series have the potential to be translated (at least semi-quantitatively) into ^{35}S input functions (Schubert et al., 2020a, 2020b, 2020c, 2020d, 2023). One of the great advantages of using ^{7}Be as proxy parameter is that ^{7}Be is one of the radio-isotopes that are measured in aerosol samples on a daily basis by International Monitoring System (IMS) particulate stations. The IMS is a global network of monitoring stations that was developed by the Comprehensive Nuclear-Test-Ban Treaty Organization (CTBTO) aiming at detecting

nuclear test explosions or nuclear accidents by continuously recording (among other signals) radionuclide data. Recently, eighty stations of the network are monitoring radioactive aerosols (among them ^{7}Be attached to aerosols). The resulting datasets are generally freely available.

2.1.4. Radio-phosphorus ($^{32/33}$P)

2.1.4.1. Natural occurrence and properties of radio-phosphorus. Phosphorus has 23 isotopes from ^{25}P to ^{47}P, with only ^{31}P being stable. The two longest-lived instable species are ^{32}P ($t_{1/2}$ = 14.3 d) and ^{33}P ($t_{1/2}$ = 25.3 d). Both are produced naturally through cosmic ray spallation of argon mainly within upper troposphere and to a lesser degree the lower stratosphere. There phosphorus oxidizes quickly to phosphate ($^{33,32}PO_4^{3-}$) and attaches to aerosols. Most of the aerosol particles are scavenged from the atmosphere by meteoric water (as $H_2PO_4^-$), transferred to the earth's surface with precipitation and finally to the groundwater. Since no natural source of radio-phosphorus exists in the subsurface, the ^{33,32}P activity concentration of the infiltrating meteoric water declines due to decay once it enters the ground.

Benitez-Nelson and Buesseler (1998) reported activity concentrations of ^{32}P and ^{33}P in rain samples collected in June and July 1996 in the state of Rhode Island, USA (41°32′ N), that varied substantially between 10.2 and 68.3 mBq/l and 9.0–64.5 mBq/l, respectively (n = 7) (Fig. 5A), however the ^{32}P/^{33}P activity ratio of 1.26 ± 0.14 (Fig. 5B) was remarkably stable. A 12-months timeseries reported by Waser and Bacon (1995) revealed activity concentrations between 2.3 and 23.7 mBq/l (Fig. 5C), also with a ^{32}P/^{33}P activity ratio that is rather constant over time, ranging around 1.0 (1.06 ± 0.16; Fig. 5D) (Note that the values originally reported by Waser and Bacon are $^{33/32}$P ratios.). The latter dataset seems to reveal slightly lower ratios during winter/spring (mean 0.99) and slightly higher ratios during summer/autumn (mean 1.12).

Phosphorus reacts readily with soil constituents, and most soils have a moderate to high capacity to bind phosphorus (e.g., Correll, 1998). This may result in low ^{32,33}P activity concentrations in groundwater. However, with continued application of excess fertilizer phosphate, the phosphate-binding capacity of agricultural soils may sooner or later become exhausted, allowing phosphate to enter the aquifer with leachate (e.g., Del Campillo et al., 1999). In the aquifer, radio-phosphorus (in the form of $^{32,33}PO_4^{3-}$) is generally mobile as a dissolved component and chemically stable over a wide range of hydrochemical conditions. However, in oxic aquifers, phosphate attenuation during transport is likely due to sorption onto iron and manganese oxide coatings covering the mineral matrix. Consequently, phosphorus is significantly more mobile under anaerobic conditions (Carlyle and Hill, 2001). Filtration of colloidal phosphorus is another form of removal from flowing groundwater (Gray et al., 2015).

2.1.4.2. Application concept for using radio-phosphorus as aqueous tracer. Even though Lal et al. (1957) already suggested using radio-phosphorus for tracing large scale air mass migration, its actual potential as

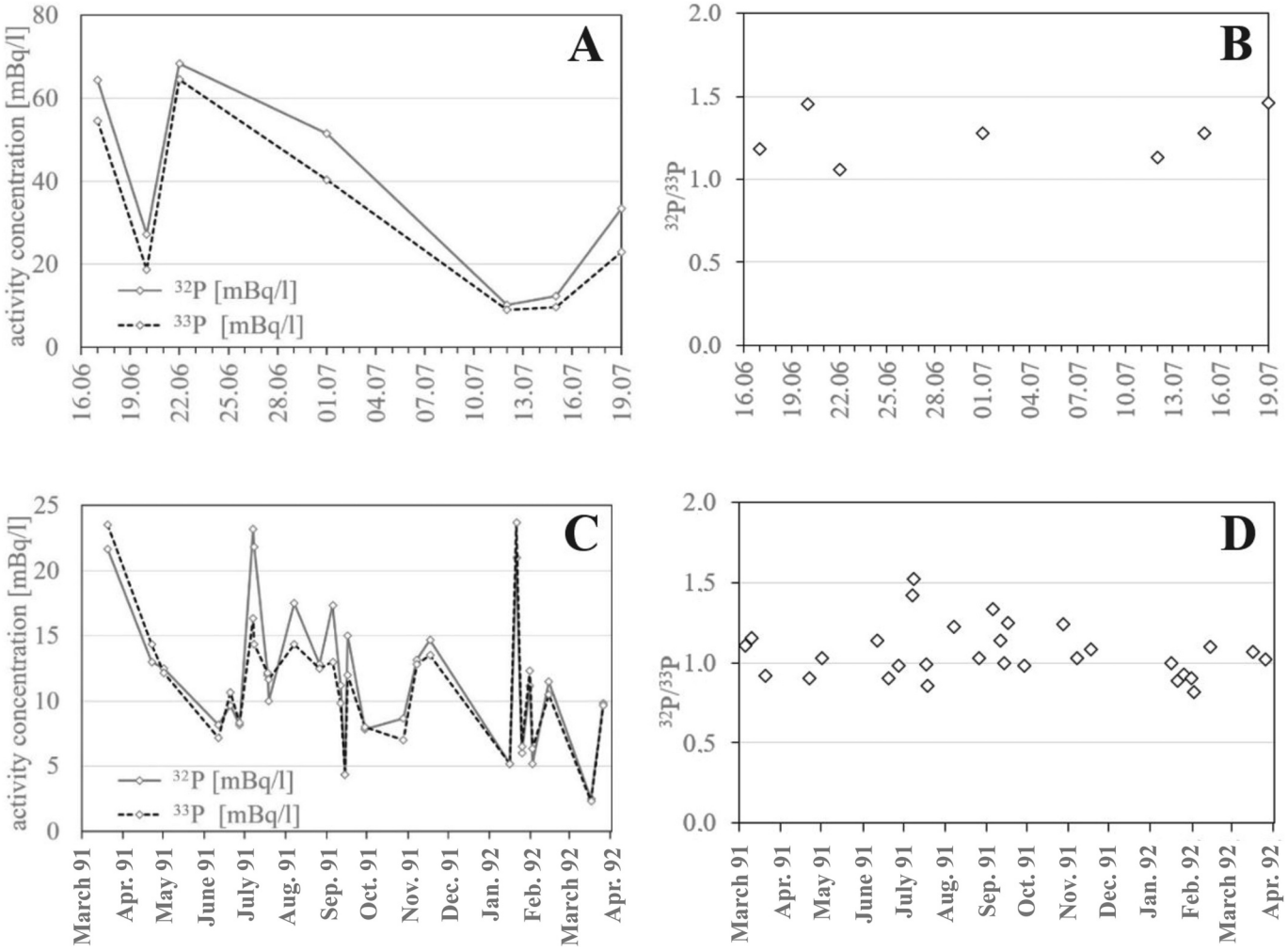

Fig. 5. ^{32}P and ^{33}P activity concentrations in rain; (A) and (B): adapted from Benitez-Nelson and Buesseler (1998); (C) and (D): adapted from Waser and Bacon, 1995 (one sample, collected on March 10th 1991, showed values that were unusual high for the region [49.3 and 42.8 mBq/l, respectively] and is thus considered an outlier).

naturally tracer wasn't investigated until about 35 years later. The first practical applications focussed on providing information on the residence time of tropospheric aerosols in the upper ocean as well as on zooplankton dynamics and phosphorus cycling within this realm (Lal and Lee, 1988; Waser et al., 1994; Waser and Bacon, 1995). Later, radio-phosphorus was also used to trace bioaccumulation of phosphorus in both aquatic biota (Smith et al., 2011) and in crops (Morel and Fardeau, 1989) and furthermore to determine stratosphere/troposphere exchange and tropospheric air mass residence times (e.g., Bhandari et al., 1970). However, to our knowledge no study yet investigated the possibility of using radio-phosphorus as groundwater residence time tracer.

In contrast to ^{35}S and ^{7}Be, the concept of using radio-phosphorous as aquatic tracer suggested here relies on an activity ratio rather than on absolute activity concentrations. Because both ^{32}P and ^{33}P are subject to the same production, transformation, and removal processes in the atmosphere, individual temporal activity variations are effectively cancelled out by using the activity ratio. The published cited above data suggests the $^{32}P/^{33}P$ activity ratio to range between ~0.8 and 1.2 with slightly higher values during summer and lower values during winter season. This implies that the use of radio-phosphorous as residence time tracer could be based on a rather simple input function or on an input value despite the varying absolute variations of radio-phosphorous in rain.

Conceptually, the ^{33}P and ^{32}P containing meteoric water enters the subsurface (with activities of $^{33}P_0$ and $^{32}P_0$), ^{33}P and ^{32}P decay is not balanced by (cosmogenic) ^{33}P and ^{32}P production anymore. Subsurface ^{32}P production by the decay of ^{32}Si ($t_{1/2} = 140$ a) is negligible. Just as ^{33}P and ^{32}P, ^{32}Si is produced in the atmosphere by cosmic ray spallation of argon and reaches the Earth's surface with precipitation. Fifield and Morgenstern (2009) report ^{32}Si activities in rain ranging between 2 and 40 mBq/m^3, which is three magnitudes below the activities that can be expected for ^{32}P.

Since ^{32}P decays about twice as fast as ^{33}P, the $^{32}P/^{33}P$ ratio in the aging groundwater decreases steadily as function of time (t) (determined by the ^{32}P and ^{33}P decay constants. The $^{32}P/^{33}P$ ratio decreases with a combined half-life $^{32/33}t_{1/2} = 33$ d (Eq. (2)).

$$^{32/33}P_t = \frac{^{32}P_0 e^{-\lambda_{32} t}}{^{33}P_0 e^{-\lambda_{33} t}} \quad (2)$$

2.1.4.3. Sampling, sample preparation and measurement of radio-phosphorus in water samples. As mentioned above, activity concentrations of ^{32}P and ^{33}P in rain vary but range generally significantly below 100 mBq/l. Thus, water sampling and sample processing for $^{32/33}PO_4$ extraction requires large volume water samples. Silker et al. (1971) (a study that was 23 years later updated by Waser et al., 1994) suggested rain water volumes of up to 60 l to be taken per sample in order to collect a sufficient amount of activity.

For radio-phosphorus extraction from the samples (after adding stable phosphate as $Na_3^{31}PO_4$ for quantification of the phosphate extraction yield) the authors utilized phosphate adsorption onto activated alumina adsorbent powder (Al_2O_3). The phosphate was desorbed from the alumina (by washing it with NaOH) and subsequently precipitated and resolved in various steps. These steps included precipitation of (i) ammonium phosphor molybdate (twice) and (ii) ammonium magnesium phosphate (also twice) to finally result in a solid $^{33,32}P$ source ready for counting on an anti-coincidence low level beta counter. Even though this detection approach allows individual counting of ^{32}P (and hence $^{32}P/^{33}P$ separation) by blocking the low ^{33}P beta emissions with an external absorber, a key disadvantage (among others) is that the efficiency of ^{33}P counting is highly impacted by self-absorption and hence strongly dependent on sample thickness and its phosphate content (Benitez-Nelson and Buesseler, 1998).

An alternative improved detection approach based on low-level liquid scintillation counting (LSC) and allowing detection of ^{33}P activities as low as 8 mBq/m^3 was suggested by Benitez-Nelson and Buesseler (1998). The related sample preparation procedure sets off with radio-phosphorus extraction by adsorption onto custom-made Fe$(OH)_3$-impregnated polypropylene adsorbers, which utilize the strong affinity of phosphorus in all its forms onto iron-coated materials. The authors impregnated polypropylene filter sheets with a $FeCl_3$ solution. For processing of freshwater samples, 30 × 2 cm PVC tubes were packed with the absorbers. The extraction yield from 25 l samples was maintained at >95 %. The authors suggested subsequent sample preparation steps for both rainwater (with virtually no stable phosphorus) and seawater (potentially high in stable phosphorus). No experiments with groundwater samples were carried out, though.

Chen et al. (2013) adapted the Fe$(OH)_3$-based extraction approach. After acidifying the water samples to pH 2 (and after adding KH_2PO_4 as extraction yield monitor) they added $FeCl_3$ and NH_4OH solution in order to precipitate Fe$(OH)_3$ as phosphorus scavenger. The phosphorus laden Fe$(OH)_3$ was then dissolved in HNO_3. The further sample processing included, as already introduced by Waser et al. (1994), precipitation steps of both ammonium phosphor molybdate and ammonium magnesium phosphate. The latter was finally dissolved in HCl and the solution loaded on a resin column to adsorb LSC-interfering cations. The resulting solution was neutralized (with NH_4OH), evaporated to dryness, taken up in deionized water and mixed with a scintillation cocktail (Optiphase HiSafe 3; PerkinElmer).

Experiments completed at the Helmholtz Centre for Environmental Research (Schubert unpublished data, 2023) showed that in particular the suggested precipitation of Fe$(OH)_3$ as scavenger is tricky since the extraction yield depends on both pH and chemical matrix of the water sample. The formation of metal-aquo complexes, i.e., compounds containing metal ions with only water as a ligand, strongly affects the precipitation behaviour in aqueous solutions. Another challenge is the quantitative separation of the Fe$(OH)_3$ precipitate, as it forms a fluffy-cloudy yellowish plume that precipitates very slowly. Hence, further research that focusses on phosphate extraction by adsorption rather than precipitation is recommended.

Two LSC measurement approaches for ^{32}P and ^{33}P in aqueous samples are applicable (Benitez-Nelson and Buesseler, 1998). Both methods use the distinctively different spectra that are produced by ^{32}P and ^{33}P, respectively, with ^{33}P emitting lower and ^{32}P higher energetic beta radiation.

The first approach is based on measuring the Cherenkov radiation. While beta-particles emitted by ^{33}P are too low-energetic to generate any Cherenkov radiation, ^{32}P emits high-energy beta-particles. The Cerenkov radiation can be detected directly by a photomultiplier without any scintillation cocktail. The authors suggest to add, in a subsequent step, a scintillation cocktail to the sample solution to determine the total radio-phosphorus activity ($^{32}P + ^{33}P$) by LSC-counting. Finally, the ^{33}P activity can be calculated by subtracting the result of the Cerenkov from the total radio-phosphorus measurement.

The second approach requires optimizing the setting of the LSC counting windows based on custom-made $^{32,33}P$ standards samples that represent the chemical composition and the quench level of the field samples. First the spectra of the standards are recorded with the LSC default settings. Based on the resulting data, counting windows for ^{33}P and ^{32}P are roughly set. The high-energy endpoint of the ^{33}P spectrum is set as high-energy channel of window A. Window B is set above window A with its high-energy channel being the endpoint of the ^{32}P spectrum. Fine-tuning of these preliminary settings is subsequently done iteratively by a series of measurements that allow optimizing the so called "figure of merit" (FOM), i.e. the ratio of efficiency squared and background (FOM = E^2/B) (Schubert et al., 2019).

2.1.4.4. Data evaluation. No study has yet been published that evaluated practically the applicability of radio-phosphorus as short-term groundwater residence time tracer. Benitez-Nelson and Buesseler

(1998) didn't compare their substantial set of rain data with radio-phosphorus activities in groundwater samples. Still, the theoretical facts summarized above suggest that natural $^{32}P/^{33}P$ can be used as short-term groundwater age tracer ratio covering a time range of about 4–5 months (based on the combined half-life of $^{32/33}t_{1/2} = 33$ d). The potentially strong retardation of phosphorus in the soil may result in only low activity concentrations in groundwater requiring large sample volumes.

The shortage of robust survey data and long-standing experiences does not allow presenting a substantiated state of knowledge regarding both the practical application of $^{32/32}P$ as age tracer and the associated data processing. In this review we highlight the potential of $^{32/33}P$ as an emerging and promising tool for groundwater research. Efforts should be undertaken by the interested scientific community to practically evaluate and communicate the potential of radio-phosphorus for the purpose.

2.1.5. *Comparing tritium (^3H) to short-lived cosmogenic radionuclides*

Compared to other cosmogenic radionuclides ^3H observations in global precipitation are abundant. Multi-decadal records are available from the Global Network of Isotopes in Precipitation (GNIP; IAEA/WMO, 2023). Still, in contrast to ^{35}S, ^7Be and $^{32,33}P$, ^3H sampled from rain, surface or groundwater does not have an unequivocal cosmogenic source tag but can be of anthropogenic or terrestrial origin, too.

The 1960s' thermonuclear bomb tests are a major anthropogenic ^3H source. Still, due to the 12.3-year half-life of ^3H, the related impact is getting less and less relevant. Morgenstern and Taylor (2009) first postulated the dissipation of the thermonuclear ^3H for the 1990s in the southern and for the 2000s in the northern hemisphere and a subsequent return to a (near-) natural steady-state regime. Recent anthropogenic emissions of tritiated water vapour originate from nuclear power generation (e.g., Köllő et al., 2011; Jefanova et al., 2018; Priebe et al., 2023), nuclear accidents (Matsumoto et al., 2013), or nuclear fuel processing (e.g., Akata et al., 2011; Schmidt et al., 2020). Industrial sources also contribute to the anthropogenic emissions (e.g., Schürch et al., 2003; Harms et al., 2016; Priebe et al., 2023).

^3H in recent precipitation can furthermore have its source in evaporation from reservoirs that contain meteoric water originating from the 1960s, such as glaciers (e.g., Di Stefano et al., 2023), permafrost (Lapp, 2015; Gibson et al., 2016; Bond and Carr, 2018; Hiyama et al., 2021), or groundwaters (e.g., Eastoe et al., 2012). The re-evaporation of continental waters furthermore alters the ^3H budget in modern-day precipitation (e.g., Tadros et al., 2014; Cauquoin et al., 2015; Mayo and Tingey, 2022). This includes water from closed sea basins, such as the Mediterranean (Juhlke et al., 2020) or the Black Sea (Rank et al., 1999; Varlam et al., 2013). Furthermore, atmospheric circulation patterns and large-scale weather situations alter ^3H in precipitation by giving preponderance to source regions (e.g., Chae and Kim, 2019) or seasons. These patterns can lead to unexpectedly high or low annual mean ^3H levels in precipitation. Duliński et al. (2019) and Terzer-Wassmuth et al. (2022a) demonstrated the latter for the Krakow and Vienna regions, respectively, which were biased low in 2015 due to relative abundance of winter precipitation and, conversely, biased high in 2018 due to intense summer rains.

Pushing aside the terrestrial (incl. the anthropogenic) influences and sources of ^3H, the highest interest in the context of short-lived cosmogenic radionuclides lies in the cosmogenic ^3H production. Spallation of ^{14}N by fast neutrons (energy >4 MeV) within the stratosphere is the most important natural ^3H source ($^{14}_7N + n \rightarrow ^{12}_6C + ^3_1H$). ^3H quickly hydrolyses into $^3H^1HO$ vapour. Ehhalt et al. (2002) demonstrated in a balloon experiment the sharp increase of stratospheric tritiated water vapour at 5–10 km above the tropopause with levels of up to 10^7 TU for measurements in the 1970s and 2 × 106 TU in the mid-1985s (more recent data is not available). $^3H^1HO$ is mainly conveyed downward by stratospheric/tropospheric exchange.

Palcsu et al. (2018) and Poluianov et al. (2020) highlighted the spatial distribution of the cosmogenic ^3H production as a function of the shielding provided by the Earth's magnetic field against the arrival of charged cosmic ray particles ("geomagnetic cut-off rigidity"). They reported the highest shielding effect over the Asian equator region and the lowest over the poles. This behaviour is reflected in spatial modelling approaches for global precipitation ^3H distributions, namely the LMDZ-iso general circulation model (GCM, Cauquoin et al., 2015) and the RCWIP-^3H predictive isocape model (Terzer-Wassmuth et al., 2022a, 2022b).

The cosmogenic ^3H production is also dependent on the 11-year cycle of the strength of the sun's magnetic field. The associated response in global post-bomb precipitation ^3H was demonstrated by Palcsu et al. (2018) for several ^3H time series in conjunction with the neutron fluxes at Oulu observatory (Finland). The authors evaluated data recorded during the solar cycles 22 (1996–2008), 23 (2008–2019) and 24 (2019-present). László et al. (2020) reconstructed the cosmogenic ^3H contribution during the thermonuclear bomb peak and the tail decades. Terzer-Wassmuth et al. (2022a, 2022b) visualized the annual mean ^3H of GNIP stations normalized by their 2008–18 mean values. The graph displayed in Fig. 6 (extended until 2022) splits northern, southern, and tropical (between the tropics of Capricorn and Cancer) stations. The variability is probably due to climatic or local influences on the precipitation ^3H. Yet, the overall variability is consistent with the recorded neutron fluxes. The variability during 2015–17 is unexplained yet but probably an overwhelming response of a climatic signal due to the reduced cosmogenic influx. The timeseries for Vienna, which is often used as *the* northern hemispheric reference curve, clearly demonstrates the susceptibility to climatic influences and therewith the challenges of adequately attributing the sources of meteoric ^3H.

A few occurrences were observed of stratosphere/troposphere exchange, which led to ^3H anomalies in snow pits in East Antarctica (Fourré et al., 2006, 2018; Hebert, 2011). This was explained by the formation of "diamond dust" enriched not only in ^3H but also ^{10}Be (Kurita et al., 2019). Qiao et al. (2021) observed similar peaks in Greenland (Camp Century ice core).

The facts summarized above indicate that ^3H and short-lived radionuclides differ in their sources and atmospheric behaviour. Still, since

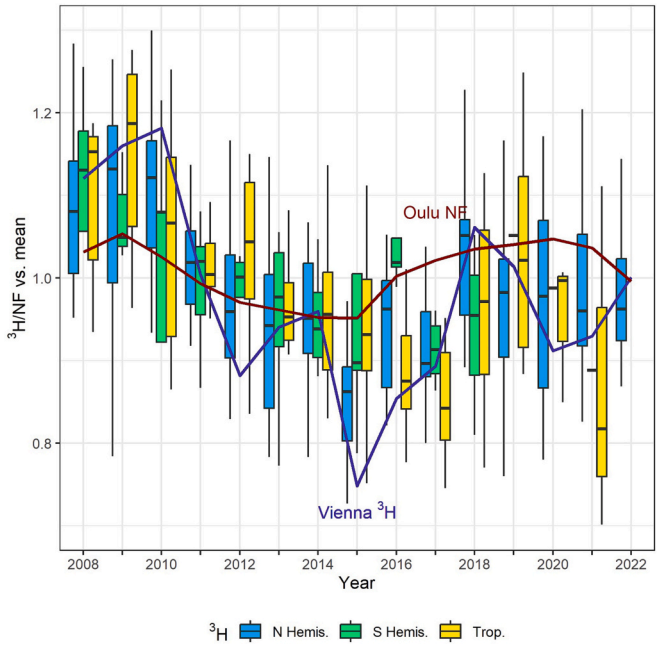

Fig. 6. ^3H of GNIP stations normalized by their 2008–2018 values split into north (blue), south (green) and tropical (yellow). The red line represents cyclical neutron fluxes, the blue line data recorded in Vienna.

^{35}S occurs mostly dissolved as $^{35}SO_4^{2-}$ in precipitation, one could expect similar patterns for the two radionuclides in precipitation, which would allow using ^{3}H as proxy for ^{35}S. There exist very few studies that report ^{35}S and ^{3}H activity concentrations in precipitation over time in the literature. Yoon et al. (2023) reported similar patterns for ^{3}H and ^{35}S. Correlation of activity concentrations in 16 precipitation samples resulted in a determination coefficient of $R^2 = 0.78$. Differences are explained by the fact that ^{3}H is part of the water molecule and therefore wouldn't be affected by aerosols in the atmosphere. Own (yet unpublished) investigations based on datasets that were collected over a 4-year period revealed a comparable result ($R^2 = 0.80$; Schubert et al., 2024). Hence, it can be presumed that even though ^{3}H is not a short-lived natural radionuclide to be applied as short-term residence time tracer in hydrogeological studies, it could be used to set up or support a regional short-lived radionuclide input function.

2.2. Short-lived geogenic radionuclides (^{222}Rn; $^{224/223}Ra$)

2.2.1. Natural radionuclides in the geosphere

The three short-lived geogenic radionuclides discussed in Section 2.2, namely ^{222}Rn (produced by ^{226}Ra), ^{223}Ra and ^{224}Ra, are part of the three natural decay chains headed by ^{238}U, ^{235}U and ^{232}Th, respectively. Different igneous rock types differ specifically in their contents in uranium and thorium and thus in radium. This rock-specific occurrence of the two elements is due to their geochemical behaviour during crystallisation differentiation of the primary magma. Due to their high valency both elements are geochemically highly incompatible (Gill, 1993). Hence, they get, during crystallisation differentiation, more and more enriched in residual magmas. As a result, they show generally depleted concentrations in basaltic (mafic) rocks (e.g., gabbro, basalt) and elevated concentrations in granitic (felsic) rock species (e.g., granite, rhyolite) and alkali feldspar rock varieties (e.g., syenite, phonolite).

The generally high uranium and thorium (and thus radium) content in granitic rocks is often bound to high mica (e.g., biotite) contents (e.g., Wollenberg, 1984; Rösler, 1984). However, mica occurs only indirectly as host mineral. The actual host is mainly zircon, which tends to occur intergrown in biotite. In the zircons, zirconium is often replaced by uranium or thorium, which makes U_3O_8 concentrations of up to 1.5 % and ThO_2 concentrations of up to 12 % possible in zircons (Rösler, 1984).

Like many other incompatible elements (e.g., Ba, Cs, Hf, K, Nb, Rb, Sr, Ta, Tl, Zr, REE), uranium and thorium are also enriched in alkali feldspar rocks. Potential host minerals here, besides zircons, include apatite, allanite, magnetite or titanite.

Further rock species that show significantly elevated concentrations in uranium and thorium are carbonatites and phosphorites. Carbonatites may contain anomalous high concentrations of incompatible elements. Besides uranium and thorium, they show the highest concentration of lanthanides of any known rock type. Phosphorite is a marine sedimentary rock that contains high amounts of phosphate minerals (up to 20 % P_2O_5). At the early stage of its formation in a reductive marine environment, U(VI) diffuses from the seawater into the organic-rich sediments where it gets reduced and precipitated as sub-microscopic (mainly uraninite) particles.

Corresponding to the elevated uranium and thorium contents in the rock types briefly introduced above, the two elements (and thus radium and radon) show also elevated concentrations in the metamorphic rocks, the sedimentary rocks as well as in the soils and sediments that derive from those by weathering. Fig. 7 illustrates the general occurrence of ^{226}Ra in some major rock types rocks.

2.2.2. Radon (^{222}Rn)

2.2.2.1. Natural occurrence and properties of radon. ^{222}Rn is the short-lived natural radiotracer that is most frequently applied in hydrological surveys. A wide range of resulting data and conclusions has been published. Most papers discuss the use of ^{222}Rn in specific case studies; some of them are exemplarily cited in the following paragraphs. Others are set up as application reviews. The latter include Adyasari et al. (2023) who discuss the use of ^{222}Rn for tracing groundwater discharge to surface waters, Sukanya et al. (2022) who talk about the application of ^{222}Rn as tracer not only in hydrogeological and but also in geological investigations and Schubert (2015) who introduces the use of ^{222}Rn as environmental tracer for assessing subsurface contamination with Non-Aqueous Phase Liquids (NAPL). We want to encourage the interested reader to take a closer look at these review papers, which allows us to abstain from repeating related details here.

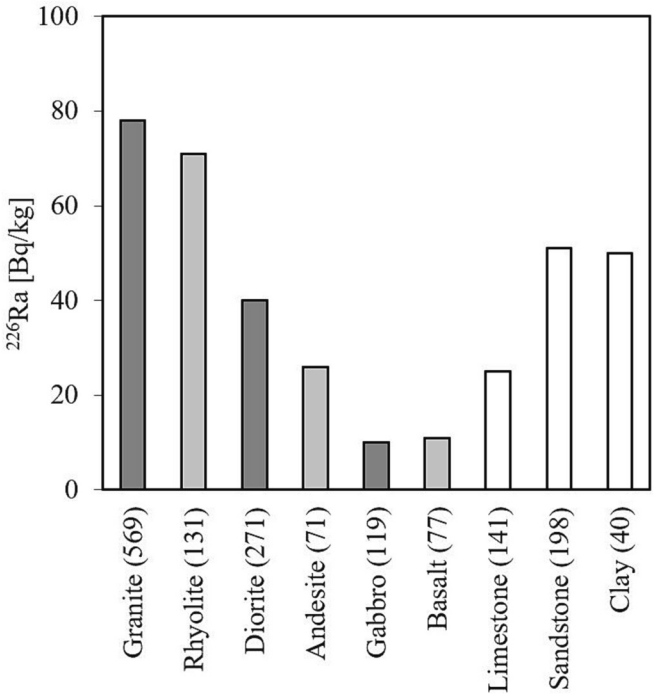

Fig. 7. Mean concentration of ^{226}Ra in rock types (after Wollenberg, 1984). The values in brackets indicate the number of samples examined. Vulcanic rocks: light grey; plutonic rocks: dark grey; sedimentary rocks and sediments: white.

As part of the ^{238}U decay chain, it is produced by ^{226}Ra decay ($t_{1/2}$ = ~1600 a) and decays itself with a $t_{1/2}$ of 3.8 days into ^{218}Po ($t_{1/2}$ = 3 min). As uranium (and thus radium) is present in all mineral matrixes of the Earth's crust (with considerably varying concentrations), ^{222}Rn is produced within the mineral grains and on grain surfaces of every aquifer and soil material (e.g., Krishnaswami and Seidemann, 1988; Nazaroff, 1992).

Part of the ^{222}Rn emanates from the mineral grains into the pore space that is filled with groundwater and soil gas, respectively. The share of the produced ^{222}Rn that reaches the groundwater-filled pore space depends mainly on the size of the aquifer mineral grains and their degree of weathering (e.g., Andrews and Wood, 1972; Wilkening, 1974; Schumann and Gundersen, 1996). In the unsaturated zone of the soil, the emanation rate into the air-filled pore space depends furthermore on the moisture content of the soil pores (e.g., Strong and Lewins, 1982; Wilkening, 1990). Generally, the ^{222}Rn emanation rate is expressed by the dimensionless emanation coefficient, which ranges for mineral materials between about 0.1 and 0.4 and can on average be assumed to amount to ~0.25 (Nazaroff, 1992). In other words, ~25 % of the ^{222}Rn produced in an average mineral matrix ends up in the pore space filled with groundwater or soil gas. Besides the emanation coefficient (ε, [/]), the equilibrium activity in groundwater or soil gas (C_{Rn}, [Bq/m^3]) depends on the ^{226}Ra activity of the mineral matrix (A_{Ra}, [Bq/kg]), its bulk

dry density (ρ, [kg/m^3]) and its pore space (n, [/]). Based on these four parameters, the C_{Rn} can theoretically be quantified (Eq. (3)). Average radon concentrations in groundwater range in general between about 5 and 50 Bq/l (but can be much higher or lower; Nazaroff and Nero, 1988).

$$C_{Rn} = \frac{A_{Ra} \times \varepsilon \times \rho}{n} \quad (3)$$

Since radon is a noble gas (no biodegradation or physical/chemical retardation must be considered; neither does it sorb or chemically interact with suspended and dissolved materials) and since anthropogenic radon sources can be excluded, it is an ideal environmental short-term tracer in hydrological studies.

2.2.2.2. Application concept for using ^{222}Rn as aqueous tracer. The ^{222}Rn tracer concept is based on the strong ^{222}Rn activity gradient between surface water and groundwater. Since ^{222}Rn is constantly produced in every aquifer matrix, any infiltrating water reaches the aquifer-specific ^{222}Rn equilibration concentration (Eq. (1)) after about 20 days (five radon half-lives). In contrast, the radon equilibrium concentration in surface waters can in general be neglected since surface waters contain only negligible amounts of dissolved ^{226}Ra and are not in contact with ^{226}Ra-bearing minerals to a relevant extent. Furthermore, ^{222}Rn rapidly degasses from surface water bodies. As a result, the ^{222}Rn activity in groundwater is on average about two to three orders of magnitude higher than in surface waters.

That results in qualitative and quantitative applications: (i) patches of elevated radon activity detected along a stream course or along the shoreline of a lake, a lagoon, or the coastal sea indicate spots or areas of groundwater discharge into the surface water body (e.g., Schubert et al., 2022); (ii) setting up a ^{222}Rn mass balance for a lake, a lagoon, a river section or a defined stretch of coastline allows quantifying the groundwater discharge into this defined surface water compartment (e.g., Petermann et al., 2018b for a lake; Petermann et al., 2018a for a lagoon; Schubert et al., 2020c for a river).

Both approaches require mapping the ^{222}Rn activity in the surface water body or the investigated section of it. The survey outcome can be limited to pinpointing the discharge spot if the terrestrial groundwater endmember cannot be determined satisfactorily (e.g., Schubert et al., 2017), if ^{222}Rn degassing from the surface water cannot be quantified adequately (e.g., Schubert et al., 2022), or if groundwater discharge quantification is of only minor interest (Montiel et al., 2019). However, if all ^{222}Rn sinks and sources can be quantified with sufficient precision, a simple radon mass balance box model can be set for the surface water body in question.

The ^{222}Rn sources include the discharging groundwater (i.e., the sought-after parameter) containing an aquifer-specific ^{222}Rn endmember concentration, ^{222}Rn diffusion from the sediment, in-situ ingrowth by decay of dissolved ^{226}Ra, upstream river inputs, and (in coastal settings or flood pulse systems) input by flood waters. ^{222}Rn sinks include atmospheric evasion ("degassing"), ^{222}Rn decay, losses by downstream river outflow, and (in coastal settings) loss by offshore mixing and ebb tides. Fig. 8 illustrates these sources and sinks.

A critical parameter for setting up a ^{222}Rn box model is the groundwater endmember. The determination of the radon activity concentration of regional groundwater inflow into the surface water body can be challenging if the local geological setting is complex (e.g., Atkinson et al., 2013; Frei et al., 2020). Since radon activities reach decay equilibrium with the aquifer matrix after about 20 days, groundwater samples for endmember determination should be taken from wells that are in the close vicinity of the investigated surface water body. The water can either be analysed as distinct samples or from a pump stream out of a well/spring using a submersible pump. If no suitable wells or springs are accessible groundwater can also be sampled by means of push point piezometers. If no or only a very limited number of adequate groundwater sampling locations are available, the ^{226}Ra activity of sediment or aquifer samples (A_{Ra}) can be determined by means of gamma spectrometry and used as proxy parameter (Eq. (3)). In this case it has to be made sure that the mineral material samples are representative for the aquifer that is hydrologically connected with the surface water body (Schubert et al., 2020b, 2020c).

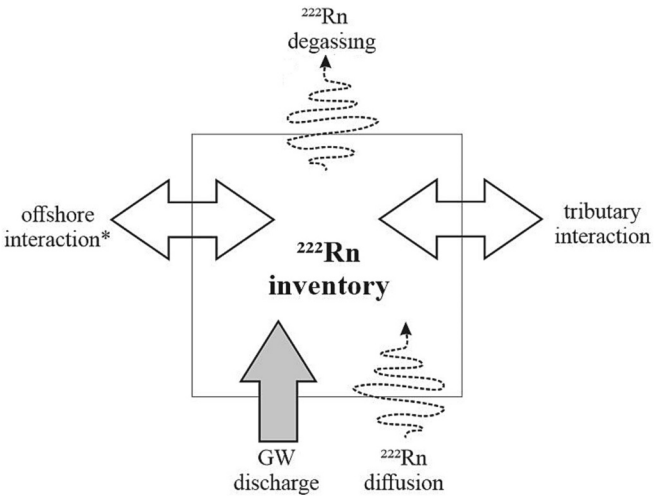

Fig. 8. Conceptual model illustrating ^{222}Rn sources and sinks for estimating groundwater discharge into surface waters. ^{222}Rn production and decay is neglected because steady state conditions are assumed. *Offshore interaction has only to be considered in coastal settings.

Diffusive radon input can be evaluated experimentally by sealing a flask filled with defined volumes of sediment and radium-free water and measuring the produced radon in the overlaying water layer after four weeks equilibration time (Corbett et al., 1998). Alternatively, Burnett and Dulaiova (2003) used an empirical relationship solely based on the ^{226}Ra activity in the sediments.

The sink that is most difficult to quantify is atmospheric evasion of ^{222}Rn from the water surface ("degassing"). Related empirical equations that are applied in most ^{222}Rn-based groundwater studies are the ones proposed by MacIntyre (1995) or Raymond et al. (2012).

Besides the briefly introduced box model approach, groundwater discharge can also be assessed based on a ^{222}Rn porewater profile assessment. While the box model is suitable for spatially and temporally integrating studies, porewater profiles are commonly used for point evaluation of groundwater discharge. The approach is based on ^{222}Rn porewater data obtained from discrete samples collected from a sediment depth profile in areas with identified groundwater seepage (Cable et al., 1996; Cable and Martin, 2008; Cook et al., 2018).

In the following three sub-sections we briefly introduce the concepts and challenges associated the investigation of groundwater discharge into (i) lakes, (ii) the coastal sea and (iii) rivers. Detailed discussions of the individual approaches are available in the cited literature.

2.2.2.2.1. Lakes. For setting up a box model for a specific lacustrine setting (Fig. 4), the investigated lake must be attributed to either of two categories: (i) well-mixed with a vertically and horizontally uniform water column or characterized by (ii) a water column with heterogeneities resultant from density/temperature stratification.

Lakes of the first category that are purely groundwater-fed represent the most straightforward setting for a ^{222}Rn single-box model approach (Schmidt et al., 2009; Schmidt et al., 2010; Dimova and Burnett, 2011; Dimova et al., 2013; Petermann et al., 2018a). Lakes with surface water inflow and outflow can also be described with a single-box model; however, the radon activities of the upstream and downstream (or flood pulse) surface waters have to be included in the mass balance (Cook et al., 2008; Burnett et al., 2017; Liao et al., 2018; Olid et al., 2022). Lakes of the second category (i.e., vertically stratified with or without surface in- and outflow) require setting up a two (or more) box model

(Kluge et al., 2007; Schmidt and Schubert, 2007).

2.2.2.2.2. Coastal sea. Quantification of submarine groundwater discharge (SGD) into the coastal sea based on the same conceptual box model approach. A related initiative that was launched in the year 2000 by IAEA and UNESCO gave rise to the first concerted studies in this regard (e.g., Burnett et al., 2006). A representative compilation of papers that discuss SGD can be found in Adyasari et al. (2023). Practically all quoted studies revealed that SGD is generally a mixture of fresh groundwater and recirculated seawater. The share of the respective contributions is governed by various hydrological processes, most importantly by tidal pumping. Burnett and Dulaiova (2003) introduced a stepwise procedure for field surveys that aim at deriving SGD rates from coastal radon inventories, including guidance on how to quantify all relevant radon source and loss terms.

In contrast to lakes, (temporally changing) offshore mixing must be considered in coastal studies (e.g., Schubert et al., 2019). That might require recording time-series of ^{222}Rn inventories in the coastal sea (e.g., Petermann et al., 2018b). Still, lateral mixing losses are hard to estimate, which might result in seemingly negative SGD fluxes (e.g., Burnett and Dimova, 2003). In coastal lagoons offshore mixing is less difficult to quantify. Here a tidal prism approach (Keulegan, 1967) can be used to calculate the net water exchange across the lagoon's inlet within a tidal cycle (Schubert et al., 2015).

2.2.2.2.3. Rivers. A literature study by Adyasari et al. (2023) revealed that groundwater contributions to the overall streamflow of rivers can vary between about 0.5 % (Agustina Campodonico et al., 2015) and 100 % (Cartwright and Gilfedder, 2015). Comparable to lakes, groundwater discharge into rivers can be investigated based on a steady state radon mass balance set up individually for sub-sections of the studied river reach (including the river flow rate as radon source/loss term).

Quantifying degassing with adapted empirical equations works reasonably well on moderate to large streams (e.g., Atkinson et al., 2013) but might become difficult in small rivulets (Schubert et al., 2020a, 2020b, 2020c, 2020d). Artificial tracer tests with gases such as helium and sulphur hexafluoride can help to quantify degassing (Clark et al., 2004; Vautier et al., 2020). For continuous measurements of air/water gas exchange Klaus et al. (2022) suggested recording underwater sound spectra to approximate contributions of turbulence and bubbles.

Furthermore, hyporheic exchange and parafluvial flow may be significant as ^{222}Rn source in river settings. In rivers increased ^{222}Rn concentrations do not necessarily indicate local groundwater inflow; the ^{222}Rn activity in the river water might be sustained by waters that are exchanged with the near-river sediments without any river water net gain. Thus, groundwater discharge can be strongly overestimated if hyporheic and parafluvial exchange are not properly evaluated and included in the mass balance (Cook et al., 2006). For assessing the impact of hyporheic and parafluvial exchange artificial tracers can be applied that allow determining volume and residence time of the water in the hyporheic zone (e.g., gases, fluorescence dyes or Resazurin; Cook et al., 2006; Abbott et al., 2016).

A suitable tool for groundwater discharge assessment that has been developed specifically to quantify groundwater fluxes into rivers is the numerical implicit finite element model FINIFLUX, a ^{222}Rn mass balance-based approach (e.g., Frei and Gilfedder, 2015; Frei et al., 2019; Schubert et al., 2020a, 2020b).

2.2.2.3. Sampling, sample preparation and measurement of radon in water samples. Radon is commonly measured directly on site applying mobile radon-in-air detectors. Hence, the radon has first to be extracted (or "stripped") from the water, i.e., either from a continuous water pump stream or from a discrete water sample. Generally, ^{222}Rn extraction from a continuous water pump stream is preferable (if applicable) because the ^{222}Rn supply in a pump stream is "unlimited" whereas a discreet sample offers only the ^{222}Rn inventory of the sampled water volume. In either case, ^{222}Rn is stripped from the water into a closed air loop that is constantly pumped through the sampled water and the detection chamber of the radon-in-air monitor with a constant pump rate (~1 l/min).

If ^{222}Rn is to be extracted from a discrete water sample, it is done by bubbling the air loop through the sample until concentration equilibrium between water sample and air loop is reached (Fig. 9A; Schubert et al., 2006). The ^{222}Rn activity measured in the air loop (C_{air}; Bq/m^3) is converted into the original ^{222}Rn activity in the water sample (C_{water}; Bq/l) by allowing for the temperature (and salinity) dependent radon partitioning coefficient (K; [/]; Schubert et al., 2012) and the volumes of air loop and water sample (V_{air}, V_{sample}, respectively; [ml]) (Eq. (4)). Generally, groundwater shows concentrations that allow sample volumes of as low as 250 ml or even less. V_{air} is given by the headspace of the applied stripping unit and the volume of the detection chamber. The temperature of the water sample is needed for calculating K based on an empiric equation published by Weigel (1978) (Eq. (5)).

^{222}Rn extraction from a continuous water pump stream is done by either spraying the water through a nozzle into a spray chamber (e.g., RAD-Aqua, Durridge; Fig. 9B; Lane-Smith and Schubert, 2020) or by pumping the water through a membrane extractor (e.g., MiniModule, 3 M™ Liqui-Cel™, USA; Fig. 9C; Schmidt et al., 2008). The ^{222}Rn concentration measured in the air loop is converted into the ^{222}Rn activity in the water pump stream by solely allowing for the ^{222}Rn partitioning coefficient, K (Eq. (6)).

$$C_{water} = C_{air}\left(\frac{V_{air}}{V_{sample}} + K\right) \quad (4)$$

$$K = 0.105 + 0.405 \times e^{0.0502 \times T(^{\circ}C)} \quad (5)$$

$$C_{water} = C_{air} \times K \quad (6)$$

^{222}Rn mapping on a lake, along a coastline, or along a river section, is

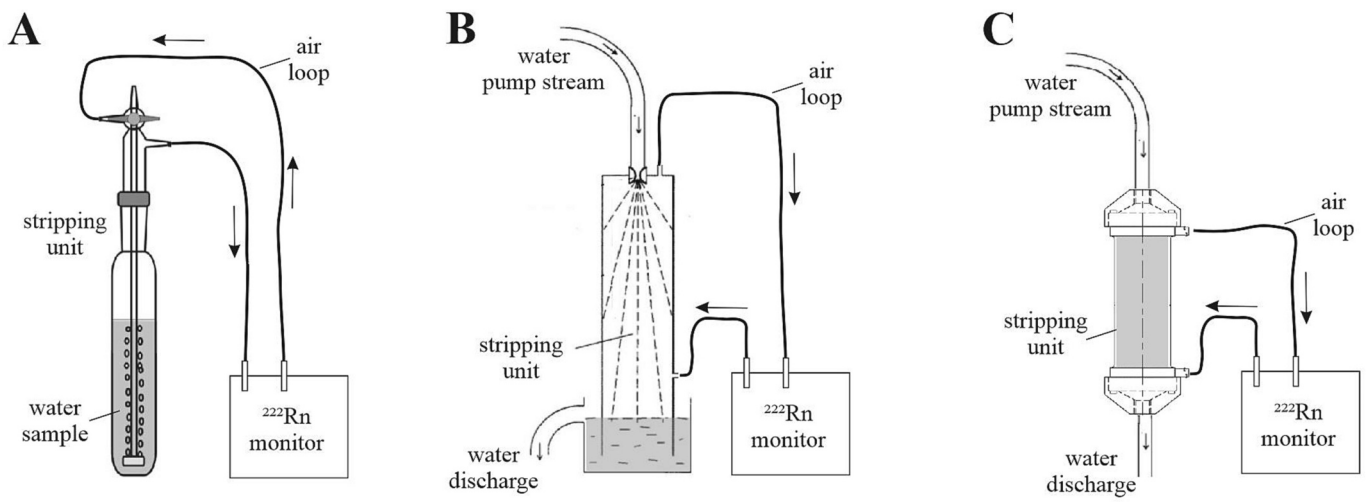

Fig. 9. Options for radon extraction from a discrete sample using a bubble module (A) and from a continuous water pump stream using a spray chamber (B) or a membrane extractor (C) as stripping unit (not to scale).

in executed from a slowly cruising vessel by radon extraction from a continuous water pump stream. For the purpose, water is pumped from about 0.5 m water depth with a rate of about 2 l/min. The mobile radon-in-air detector is set to an appropriate counting cycle (e.g., ~10 or ~ 15 min). Counting cycle and cruising speed (preferably ~4 km/h) determine the profile length that is covered with each ^{222}Rn reading. To improve statistical reliability of the results two detection setups (two water pumps, two stripping units and two radon monitors) can be run in sequence or in parallel.

Two types of radon-in-air monitors exist. One type uses a pulse ionization chamber ("PIC") (AlphaGuard, Bertin Instruments, Germany); the other relies on a passivated solid-state ion-implanted planar silicon ("PIPS") alpha detector (RAD8, Durridge, U.S.A.). Whereas the practical handling of the two detector types is comparable, their detection concept is fundamentally different.[1]

If no mobile radon-in-air detector is available or in the case of limited sample water volumes (e.g., porewater samples), ^{222}Rn can also be measured in the laboratory using a liquid scintillation counter (LSC). For LSC measurement the ^{222}Rn has to be transferred from the water sample into a scintillation cocktail. An established method involves injection of a 10 ml water sample into a 20 ml LSC vial preloaded with 10 ml scintillation cocktail (e.g., Prichard and Gesell, 1977; Cantaloub et al., 1997). If low radon-in-water concentrations are to be analysed, radon extraction from larger water volumes might be required. A related

[1] Counting radon decays with a PIC detector makes use of the ionizing nature of alpha radiation. The detection chamber consists generally of a cathode cylinder with a coaxially located internal anode wire. A voltage potential is applied between the two electrodes to create an electric field (ca. 750 V DC). Each radon decay within the chamber ionizes air molecules (N_2, O_2). The resultant cluster of positive ions and dissociated electrons moves to the respective electrodes. This generates an output signal, which is measured as a continuous ionization current. As a consequence, alpha decays within the PIC (i.e., radon decays) are counted directly without any delay. The time-lag between a change in radon activity in the "stripped" water and the counting signal is solely determined by the water/air equilibration time in the stripping unit. A disadvantage of PIC detectors is, that the energy of different types of radiation (e.g., resulting from different radionuclides) cannot be differentiated.In contrast, the PIPS detector does not count radon decays directly but the decay of the radon progeny ^{218}Po and ^{214}Po. The detection concept can be summarized with "electrostatic precipitation of short-lived radon progeny, followed by high-resolution alpha spectrometry" (Sadler, 2023). Within the detection chamber nearly each decaying radon atom (in fact, 88 % of them; Hopke, 1996) produces a positively charged ^{218}Po ion, which is drawn to the negatively charged cathode by an electric field (ca. 2500 V DC). There it sticks until it decays with a half-life of about 3 min, thereby generating an output signal. Decay equilibrium between radon in the detection chamber and ^{218}Po on the detector is reached after five ^{218}Po half-lives. That implies that the actual radon concentration in the detection chamber (air loop) is detected with a delay of about 15 min. (A second output signal results from the decay of ^{214}Po. However, this signal is delayed by about 2.5 h based on the 27 min half-life of ^{214}Pb.) Still, the 15 min delay of the output signal is in most cases of only minor relevance as the time taken to reach water/air equilibration in the stripping unit is usually in the same range. On the other hand, the advantage of a PIPS detector is that it distinguishes, on an event-by-event basis, counts from radon (^{222}Rn) progeny from those from thoron (^{220}Rn) progeny, and distinguishes also the short-lived progeny species (^{218}Po, ^{214}Po) from the long-lived species that cause a build-up of background over time in PIC instruments (^{210}Pb, ^{210}Po).

sample preparation and measurement protocol was introduced by Freyer et al. (1997) and optimized by Schubert et al. (2014). In case of laboratory analysis of water samples, it has generally to be kept in mind that samples must be transported promptly to the laboratory for analyses to minimize ^{222}Rn decay loss.

No matter what approach for ^{222}Rn measurement is chosen it has to be kept in mind that ^{222}Rn strongly partitions into air. Therefore, all water sampling must be done carefully avoiding bubbling or water turbulence while sampling. If a groundwater monitoring well is sampled the well should be fully purged before sampling to avoid sampling stagnant well water.

2.2.2.4. Data evaluation. If the sole localization of groundwater discharge spots is the purpose of a study, a simple outlining of local ^{222}Rn maxima in the surface water is the adequate means. Spatial ^{222}Rn surveys produce maps that reveal diffuse groundwater inputs or concentrated discharge hotspots (e.g., Montiel et al., 2019). For the quantitative assessment of groundwater discharge rates (and, resultingly, water residence times of lakes) quantitative data evaluation is required for setting up the ^{222}Rn mass balance (Fig. 4). Uncertainties in setting up a radon mass balance result in corresponding uncertainties in the final results. The individual relevancies of the parameters are highly dependent on the site-specific hydrogeology, morphology and meteorological influences. More details related to the issues discussed above have been outlined in a large number of related studies. A comprehensive summary reflecting all related advantages and challenges is also given by Adyasari et al. (2023).

2.2.3. Short-lived radium ($^{224/223}$Ra)

2.2.3.1. Natural occurrence and properties of radium. The three natural decay chains include four naturally occurring radium isotopes, namely ^{224}Ra, ^{223}Ra, ^{228}Ra and ^{226}Ra, which are produced by alpha decay of the thorium isotopes ^{228}Th, ^{227}Th, ^{232}Th and ^{230}Th, respectively. The radium isotopes, in turn, are decaying with half-lives of 3.6 days (α), 11.4 days (α), 5.8 years (β) and 1600 years (α), respectively. The production rate of the individual radium isotopes depends on the associated thorium contents of the mineral matrix. Since uranium and thorium, which are heading the natural decay chains, are present in all rock species of the Earth's crust, the four natural radium species are ubiquitously present in any soil and sediment (Section 2.2.1). Of interest in the given context are the two short-lived species ^{224}Ra and ^{223}Ra. Like ^{222}Rn, groundwater is generally enriched in dissolved radium in comparison to surface waters. There are no noteworthy anthropogenic radium sources and dry or wet radium deposition is generally negligible.

Generally, the radium activity in groundwater is determined by the radium sources present in the aquifer. These sources include (i) thorium decay within the aquifer mineral grains, (ii) radium release from the mineral grains by either (ii-a) recoil or (ii-b) weathering, as well as (iii-a) desorption of radium from the grain's surfaces. The radium sinks include (iii-b) radium adsorption onto the mineral surfaces, (v) co-precipitation with major hydroxides, carbonates or sulphates, and (iv) decay of the dissolved radium.

Regarding the short-lived isotopes (^{223}Ra and ^{224}Ra), both radium mobilization by weathering and radium loss by co-precipitation play negligible roles. Radium loss by decay can be quantified straightforwardly based on the decay equation (Eq. (1)) and the respective decay coefficients. The remaining sources and sinks that can neither be neglected nor easily determined shall be briefly discussed in the following.

(ii) The radium production rate within the mineral grains depends on the thorium activity of the aquifer matrix and hence on the matrix type (granitic, basaltic etc.; Section 2.2.1). Related guiding values can be found in the literature (Nazaroff and Nero, 1988; Ivanovich and Harmon, 1992) or determined by means of gamma spectrometry. All four radium species show either distinct gamma lines (^{223}Ra, ^{226}Ra) or produce short-lived progeny with distinct gamma lines (^{228}Ra, ^{224}Ra, ^{226}Ra).

(iii) Radium release by recoil from the mineral matrix is a function of the surface area and the surface characteristics of the aquifer grains. The greater the surface/volume ratio, the greater the fraction of the produced radium that is finally released into the groundwater by recoil (Beck and Cochran, 2013). Weathering forces that increase of the inner surface of a sediment is fostering radium release by recoil on the long-term.

(iiii) The degree of radium adsorption/desorption onto matrix surfaces depends (besides the available surface area) on two parameters, namely the cation exchange capacity of the mineral material and the ionic strength of the groundwater, i.e., its salinity (Beck and Cochran, 2013). High ionic strength hampers radium adsorption due to competition with other dissolved cations such as Na^+, K^+, Ca^{2+}. The matrix properties regarding radium adsorption/desorption are commonly quantified with the distribution coefficient K_D (Eq. (7)). Matrix-dependently, K_D values range over several orders of magnitude from 10^{-2} to 10^2 m^3/kg (Beck and Cochran, 2013).

$$K_D\ \left[m^3/kg\right] = Ra_{adsorbed}\ [Bq/kg] / Ra_{desorbed}\ \left[Bq/m^3\right] \quad (7)$$

2.2.3.2. Application concept for using the $^{224/223}$Ra ratio as aqueous tracer. The application concept for using the $^{224/223}$Ra ratio as tracer in groundwater/surface water interaction studies is based on the distinct radium concentration gradient between hydraulically connected groundwater and surface water bodies. The half-lives of the two nuclides result in a decrease of the (unsupported) $^{224/223}$Ra activity ratio with a combined half-life of 5.35 days. Hence, the $^{224/223}$Ra activity ratio detected in surface water can be used as short-term water age indicator ("radium age") as it is a measure of the mean residence time of porewater that was freshly discharged from groundwater/porewater to surface water (Moore, 2000; Burnett et al., 2008; Garcia-Orellana et al., 2021).

Due to the high tendency to adsorption in freshwater systems (and considering an exemplary groundwater flow of 1 cm/d) all four radium isotopes would reach equilibrium within a distance of only a few centimetres in fresh groundwaters. In saline systems, on the other hand, the required flow path lengths would be on the order of tens of cm for ^{223}Ra and ^{224}Ra, around 1 m for ^{228}Ra and around 500 m for ^{226}Ra (Garcia-Orellana et al., 2021). Hence, only few studies applied radium isotopes in freshwater environments (Molina-Porras et al., 2020; Diego-Feliu et al., 2021). Diego-Feliu suggested an advective transport model that integrates ^{224}Ra, ^{228}Ra, ^{226}Ra, and radon and their immediate parents to calculate groundwater transit times.

2.2.3.3. Sampling, sample preparation and measurement of $^{224/223}$Ra in water samples. Using an activity ratio as water age indicator makes no detection of absolute activity concentrations required. The key requirement is rather to collect a sufficient volume of water for the determination of statistically reliable $^{224/223}$Ra count rates.

For determination of the $^{224/223}$Ra activity ratio in water samples, the radium has to be extracted from the water. This is commonly done by means of MnO_2-impregnated acrylic fibres (Moore, 1976). If a well is sampled (e.g., for groundwater endmember definition) the fibre is placed into a flow-through cartridge and the water is pumped through the cartridge with a pump rate of about 1 l/min (Moore and Reid, 1973). The radium that is dissolved in the water pump stream is quantitatively adsorbed by the fibre. In order to collect an amount of $^{224/223}$Ra activity that is sufficient for the statistically reliable definition of a groundwater endmember, groundwater volumes of up to 100 l should be extracted

(Rocha et al., 2015).

There are two options for sampling $^{224/223}$Ra from a surface water body. As a first option, moorings can be placed at defined points reasonably distributed in the surface water body of concern, such as in a lagoon or a stretch of coastline, with the MnO_2 coated fibres contained in mesh bags that are attached to the moorings about 1 m below the water surface. To allow the adsorption of a sufficient amount of radium, the mesh bags should stay in the water for at least 24 h (Moore, 1976). A second option is to collect distinct water samples (recommended are at least 60 l), which are subsequently pumped through flow-through cartridges as described for the well sampling.

Due to the short combined $^{224/223}$Ra half-live, the radium-laden fibre samples should be analysed a few days after sampling (and correcting the data for the time since collection). In most published studies ^{224}Ra and ^{223}Ra activities collected by using MnO_2 fibres are determined by means of a Radium Delayed Coincidence Counter (RaDeCC). The RaDeCC has been developed by Moore and Arnold (1996) (Diego-Feliu et al., 2020) and is basically an alpha detector system that allows a straightforward, robust and rapid determination of the short-lived ^{223}Ra and ^{224}Ra based on a design introduced by Giffin et al. (1963). For sample preparation, the MnO_2 fibres are simply washed with radium-free tap water and subsequently partially dried (with compressed air) to remove excess water. Thereafter, the samples are measured for ^{223}Ra and ^{224}Ra by counting the respective short-lived radon daughters (^{219}Rn and ^{220}Rn, respectively) in a closed circulating helium loop.

2.2.3.4. Data evaluation. The $^{224/223}$Ra activity ratio of the investigated surface water that was brought in touch with the MnO_2 fibres is a measure of the time elapsed since the water was discharged from the aquifer or sediment matrix, i.e., since it was isolated from the radium source (Moore, 2000). The approach assumes that the $^{224/223}$Ra ratio of the groundwater endmember is timely and spatially invariant for the investigated surface water body and that sources or sinks of radium in the surface water body (once the water has left the aquifer) are limited to (off-shore) mixing and radioactive decay. The time elapsed since the groundwater left aquifer or sediment can be determined by solving Eq. (8) for t (Eq. (9)),

$$^{224/223}AR_{measured} = {}^{224/223}AR_{endmember} \times e^{(\lambda 223 - \lambda 224)\times t} \quad (8)$$

$$t = \frac{ln\left(\frac{AR_{SGD}}{AR_{EM}}\right)}{(\lambda_{223} - \lambda_{224})} \quad (9)$$

where AR represents the $^{224/223}$Ra activity ratio of the seawater sample (AR_{SGD}) and of the groundwater endmember (AR_{EM}), λ the decay constant for the respective radium isotope (^{223}Ra: 7.019 * 10^{-7} s^{-1}; ^{224}Ra: 2.209 * 10^{-6} s^{-1}) and t the elapsed time (the "radium age") (Petermann et al., 2018a, 2018b; Rocha et al., 2015). If no groundwater endmember is available or if the geological situation is too complex to define a reliable value, the highest $^{224/223}$Ra ratio detected in the surface water can be defined as initial value, i.e., as representative for sediment porewater freshly discharged into the surface water body (Schubert et al., 2023).

Because radium is preferentially adsorbed onto mineral grains, the time to reach concentration equilibrium between a freshly recharged groundwater (i.e., percolating meteoric water or infiltrated surface water) and the aquifer matrix (defined as "bulk radioactive equilibrium" by Diego-Feliu et al., 2021) is more difficult to estimate as for the noble gas radon. However, for groundwater endmember definition this time needs to be understood in order to assess the degree of radium equilibration in groundwater since aquifer recharge. Besides the groundwater flow velocity, the equilibration time determines the groundwater flow distance that is required to reach concentration equilibrium. Related models are generally based on the assumption that the radium exchange between mineral matrix and groundwater principally occurs via ion exchange, neglecting the processes of weathering or precipitation (Diego-Feliu et al., 2021). Hence, the equilibration time strongly depends on the characteristics of the aquifer, namely on the distribution coefficient K_D (Eq. 7) as well as on the half-life of the individual radium isotope (Krishnaswamie et al., 1982; Beck et al., 2013). Generally, it can be stated that (i) the equilibrium time decreases as K_D increases and (ii) the equilibrium time ranges from minutes to hours for the short-lived ^{224}Ra and ^{223}Ra, from hours to days for ^{228}Ra, and from days to years for ^{226}Ra (Garcia-Orellana et al., 2021). Equilibrium times can be converted to equilibrium distances by assuming a constant flow groundwater velocity through the aquifer in question.

Applying Eq. (8), all collected $^{224/223}$Ra ratios are transferred into radium ages representative for the sampling locations. The resulting data represents the mean apparent water ages of the discharged groundwater at the locations either collected over a 24-h exposure time (mooring approach) or as distinct samples (distinct sample approach). The combined $^{224/223}$Ra half-life allows dating apparent water ages of about up to three weeks. Generally, the maximum mean water age revealed in a surface water body allows estimating the intensity of the tidal flushing of a lagoon or a coastal section.

3. Discussion - exemplary applications for joint tracer data interpretation

3.1. Vulnerability mapping of aquifers

As mentioned in Section 1, shallow aquifer vulnerability assessment is a key application of the short-lived tracers discussed in this paper. Generally, an aquifer is considered vulnerable to anthropogenic pollution when groundwater recharge is happening recently or has happened in the recent past. The related groundwaters dating is usually done based on tritium, CFCs or SF_6 data (Jurgens et al., 2022). Still, since an aquifer is the more vulnerable the more sudden contamination spills of the groundwater are likely, the time frames covered by the named tracers is in many cases not appropriate. In the context of this paper, we discuss tracer approaches applicable for assessing the vulnerability of aquifers that are potentially exposed to sudden pollution spills, i.e., very young groundwaters.

Short water residence time investigation is furthermore of key interest for studying the removal of bacterial faecal indicators from recharging water. Sprenger et al. (2011) point out that during flood periods, riverbank filtration systems must be considered as highly vulnerable to pathogen contamination due to shortened travel times. Wang et al. (2022) reported that in such systems residence times as low as ten days proved to be sufficient to clean the water from pathogens.

Another example for the necessity of understanding short-term recharge processes is aquifers in fractured bedrock settings. Many index-based methods, such as the very frequently used DRASTIC model (Barbulescu, 2020) generally underestimate the vulnerability of fractured bedrock aquifers, which requires further investigation and development of indices that are suitable for this aquifer type (Wei, 1998). Generally, fractured rock aquifers represent challenges for residence time investigations, as hydraulic conductivity and effective porosity are more complicated to be correctly determined. In many regions, well developed karst aquifers, which are characterized by fast flow paths and low retention times of contaminants originating at the surface (Savoy et al., 2011; Harjung et al., 2023), represent the main source of drinking water (Hartmann et al., 2021).

In this context it shall be pointed out, that the terminology "groundwater age" is often not appropriate as most groundwaters in shallow and/or fractured aquifers show a dynamic age range. Suckow (2014) discussed in detail that for groundwater an "age" cannot be determined (although it is a useful "zero-order concept" abundantly used). The term "mean residence time" is in general more adequate (Suckow, 2014). For water resource managers it is important to know not only the average groundwater age but to get information about the

youngest portion of the age spectrum and hence about the vulnerability of the resource. A qualitative proof of the presence of recent meteoric waters, e.g., as result of dynamic recharge triggered by specific hydrological conditions, is thus very valuable.

Even for investigating deep and/or artesian aquifers, short-lived radioisotopes represent a promising addition to the conventional tracer suite as they allow to prove/disprove the presence of very young water and hence to evaluate the integrity of well casings (supplementary to geophysical methods and borehole camera surveys) (Somaratne et al., 2013).

Generally, it can be stated that using multiple tracers with different concentration vs. residence time relationships and different behaviours regarding their retardation within the subsurface, is important if residence times and recharge rates in highly vulnerable aquifers are to be realistically estimated. For example, groundwater residence times and ages estimated based on stable water isotope and radio-sulphur data differ from those based on tracer gas data ("gas chronometers"). While the former data reflects also the time and processes taking place in the unsaturated zone, gas chronometers only start counting as the water reaches gas confinement, i.e., below the groundwater table (Plummer et al., 2001). Since the residence time of percolating waters in the unsaturated zone is important as many biogeochemical processes take place there, only the combination of tracers, which allows to account for travel times through the different hydrological domains, is appropriate for the purpose.

Burns et al. (1998) found results from stable water isotopes in agreement with age ranges calculated from ^{35}S, considering that (i) stable water isotopes are monitored usually over longer time scales, which averages out certain short-term events and (ii) the input function for ^{35}S can be highly variable (Schubert et al., 2020a, 2020b, 2020c, 2020d). Still, the application of just a single tracer might lead to wrong conclusions. ^{35}S, for instance, might get retarded in the unsaturated zone by uptake and exchange of sulphate in plants and soils (Novák and Přechová, 1995; Plummer et al., 2001). Anoxic environments could add another layer of complexity due to sulphate reduction (Harris et al., 2006). Constraining such biogeochemical cycling of sulphate could possibly be achieved through stable isotopes of sulphate $\delta^{34}S$ and $\delta^{18}O$ (Kester et al., 2003).

For the quantification of groundwater travel times up to three weeks, the combination of conventional artificial tracers with ^{222}Rn can be valuable. Based on the initial radon disequilibrium, it is possible to understand the timing of fresh groundwater recharge. This geochronometer is limited to a maximum of about 20 days as the activity concentration of the recharged water approaches equilibrium in the aquifer after five ^{222}Rn half-lives. For example, using ^{222}Rn as tracer Snow and Spalding (1997) found flow pathways and residence time estimates that were consistent with bromide tracer breakthrough times in wells.

A further application is vulnerability assessment of springs to nuclear disasters and industrial accidents. Using short-lived cosmogenic radioisotopes for the purpose allows water resource managers to identify springs or wells that might become unusable for drinking water supply in cases of nuclear disasters or industrial accidents. Two related studies were executed in the Eastern Alps, Austria (Kralik et al., 2016).

In the first study, water sampling for ^{35}S was performed on a site in the dolomitic Alps, where many tracer tests (incl. fluorescent tracers, $\delta^{18}O/^{2}H$ and $^{3}H/^{3}He$) had already been performed. Four rain samples and six spring water samples were collected between March and May 2013 and between July and October 2014. Rainwater was sampled as composite samples at a meteorological station located about 900 m asl. Spring water was collected from two springs, one hydraulically connected to a fault zone and one fed from a matrix aquifer, both located about 500 m asl. All four rain samples showed noteworthy ^{35}S activities, with significantly higher values recorded in July–October (42.5; 58.4 mBq/l, respectively) compared to March–May (12.5; 24.2 mBq/l, respectively). The data supported the concept of generally elevated ^{35}S activities in rain during the summer months (Schubert et al., 2020a). The results associated to the two springs differed. On the one hand, ^{35}S was detected in the samples taken from the fault zone spring (activity concentrations between 0.8 and 3.3 mBq/l) indicating shares of sub-yearly groundwater. On the other hand, ^{35}S activity was only detected in one of the samples taken from the matrix spring (1.8 mBq/l). The matrix spring is uncased and the sample containing measurable ^{35}S was taken after a heavy rain event, and therefore, reflecting surface water runoff. As a result, only the matrix spring was found to tap a reservoir of low vulnerability. These results were consistent with the conceptual understanding of the springs.

In the second study, executed on the western end of the European Eastern-Alps, one meteorological station and eleven springs and wells were sampled for ^{35}S. All eleven springs and wells were expected to produce non-vulnerable water with a residence time between 10 and 40 years. Again, the overall purpose of the study was to prove/disprove the presence of shares of "very young" groundwater (<1 year) in the spring/well discharge. The results revealed (besides a ^{35}S activity in rain of 49.3 mBq/l; July 2014) in two of the sampled wells detectable ^{35}S activities (1.1 and 4.6 mBq/l; Kralik et al., 2016) indicating shares of sub-yearly meteoric water. Consequently, these two wells were excluded from the group of wells to be used for emergency drinking water supply after a major accident.

Summarizing it can be stated that the integration of short-lived radioisotopes into multi-tracer applications can be recommended for a wide variety of aquifer vulnerability assessment studies. Only combining several tracers that are sensitive to a range of residence times and processes can reduce uncertainties in quantitatively assessing the age structure of a shallow groundwater.

3.2. *Semi-quantitative process assessment at managed aquifer recharge sites*

Managed Aquifer Recharge (MAR) is a water management approach to increase local potable groundwater supplies. It was first used in coastal dunes in the Netherlands and is currently employed throughout the world. The dating of artificially recharged groundwater near MAR facilities can be done by applying a multi-tracer application including ^{35}S.

In the state of California, USA, water agencies are required to determine travel times of artificially recharged groundwater to the production wells for health reasons. Knowing that the travel time is <1.2 years allows the water agencies to comply with the state regulations. Because of its short half-life, ^{35}S is an ideal tracer to determine such short travel times and therefore whether or not a MAR facility is complying with the regulations. The ^{35}S method was used at a MAR site in Southern California, namely at the Kraemer Basin MAR site, Orange County (Urióstegui et al., 2016).

Kraemer Basin is one of five MAR ponds, which are in operation since the late 1990s and which are a source of groundwater recharge in the Orange County Groundwater Basin. Additionally, a 10-km reach of the Santa Ana River is also used. In total, these recharge sites provide ~70 % of the water demand for 2.5 million inhabitants of the region. Groundwater flow from the Kraemer Basin MAR site has been studied for decades using a number of geochemical techniques including $^{3}H/^{3}He$ dating and tracer experiments with both ^{136}Xe and SF_6 (e.g., Clark et al., 2004; Clark et al., 2014). In the vicinity of the Kraemer Basin MAR pond, groundwater can be sampled from a number of monitoring wells, some of them allowing sampling from different depths. Results from these geochemical studies allowed mapping the plume of MAR water. The application of ^{35}S as supplementary tracer was intended to additionally reveal information on the apparent water ages, i.e., on the water travel times from the pond to the production wells.

As a result of the study it could be shown, that travel times vary in different depth of the aquifer. The ^{35}S activities detected in the groundwater sampled from the production wells verified semi-

quantitatively groundwater ages above 1.2 years. Still, a more quantitative data interpretation proved challenging. As one cause of the difficulties the authors assumed an unidentified low SO_4/high ^{35}S source. They considered the possibilities of either an anthropogenic source (as assumed by Schubert et al., 2020a, 2020b, 2020c, 2020d) or a strong short-term intrusion of stratospheric air as reported by Lin et al. (2016). Another problem for quantitative data interpretation might have been the summer stratification of the MAR pond. Summarizing, it could be stated that while the Kraemer Basin ^{35}S study did not result in a quantitative travel times distribution pattern, it did answer the question if the MAR water travel times at the site are >1.2 years. This semi-quantitative result allowed conclusions on whether or not the MAR facility follows the state regulations.

3.3. Investigation of groundwater/surface water interaction

A central issue in water resource management is the recognition of the many links between groundwater and surface waters (including rivers, lakes, wetlands, estuaries and coastal seas) and the appreciation of the relevance of these interactions. The complex water flow and nutrient exchange processes at the groundwater/surface water interface at various scales collectively come under the denomination of "groundwater/surface water interaction" (GSI). The exchange processes have tremendous impacts on both water quantity and quality and call hence for specifically tailored investigation approaches that allow localizing and quantifying GSI with the aim to evaluate the related impacts and responses. Prominent fields of GSI research include (i) the overexploitation of coastal aquifers, causing seawater infiltration and aquifer salinization, and (ii) the discharge of contaminated groundwater into surface waters leading to their pollution and eutrophication.

A sound evaluation of the timing and extent of hydrological interactions between catchment components can only be achieved by combining tracer methods that individually allow investigating flow path and residence times. The information that results from such multi-tracer approaches have the potential to reveal intra- and trans-catchment connections as it allows tracing from where and when water (and dissolved matter) is coming from (Abbott et al., 2016; Kralik et al., 2016). As an example, submarine groundwater discharge (SGD) into coastal lagoons shall be briefly discussed.

Coastal lagoons are generally vulnerable habitats that host fragile marine ecosystems. At the same time, they are often threatened by nutrient-laden SGD. The localization of SGD spots and the quantification of the associated water and matter flux rates are therefore of central interest. The standard water parameters electrical conductivity (EC) and pH as well as stable water isotope signatures (δ^2H, $\delta^{18}O$) have proven suitable as indicators in this regard. However, while distribution patterns of EC, pH and $\delta^2H/\delta^{18}O$ in coastal lagoons reveal freshwater discharge in general, a separation between discharging surface water and SGD is not possible. ^{222}Rn is the tracer of choice here. A case study executed in a bay in Western Ireland aimed to evaluate the informative value of the named parameters in locating and quantifying SGD (Schubert et al., 2015). The results revealed that ^{222}Rn is the most sensitive of the parameters applied for SGD detection. However, only their combined evaluation allowed a separation of groundwater and surface water contributions to the overall freshwater discharge into the lagoon.

In case of lagoons or estuaries that are highly impacted by evaporation stable water isotope and EC data are also of limited (or no use at all). In a study executed by Schubert et al. (2023) only the joint evaluation of ^{222}Rn, EC and stable isotope datasets allowed locating and quantifying SGD. The set up ^{222}Rn mass balance was supported by $^{224}/^{223}Ra$ as supplementary tracer ratio, since radium is not impacted by evaporation nor degassing. Besides indicating SGD spots, the $^{224}Ra/^{223}Ra$ ratio analysis allowed revealing information on the apparent residence time of the discharged groundwater within the lagoon and hence on the lagoon's flushing intensity.

Radium isotopes have been used in a wide range of groundwater/seawater interaction studies. Radium activity concentrations in coastal groundwater are elevated due to the continuous circulation between fresh terrestrial groundwater and saline coastal seawater within the subterranean estuary, mainly driven by marine forces (tides, waves and storms). In fact, ^{224}Ra was (in combination with ^{226}Ra and ^{228}Ra) first applied as tracer in estuarine mixing studies, which require covering process time-scales of up to ten days (Elsinger and Moore, 1983). Furthermore, Moore (2000) executed benchmarking studies on the use of ^{223}Ra and ^{224}Ra for setting up conceptual models to estimate apparent ages of coastal waters and coastal water mixing rates. Rama and Moore (1996) used the four natural radium nuclides (the "radium quartet") for the first time as SGD tracers, initiating thereby numerous related studies (e.g., Burnett et al., 2001; Burnett et al., 2006; Ma and Zhang, 2020). A representative selection of related papers has been compiled by Garcia-Orellana et al. (2021).

3.4. Catchment hydrology

The pathways and timing of water to become streamflow are in the focus of catchment hydrology. However, the tools to evaluate these characteristics for a catchment in the past and to predict them for the future are diverse. Metrics such as the runoff coefficient or the separation of the hydrograph into base-flow and quick-flow can provide important insights of the functioning of a catchment.

Hydrograph separation is a technique to understand the temporal and/or geographic origin of streamflow. Hydrometric information is often combined with tracer data, whereby the selection of the type of tracer(s), the number of tracer(s), and the characterization of the end-member(s) is critical for the application: some end-members and tracers may lead to multiple mathematically possible solutions that don't represent the physical processes correctly (Bansah and Ali, 2017). In fact, a joint evaluation of the data is often required to understand all contributions to streamflow (Barthold et al., 2011). For further information on hydrograph separation using stable water isotopes the reader is referred to Klaus and McDonnell (2013) and Penna and van Meerveld (2019).

Water stable isotopes showed that the response of a catchment to a precipitation event is dependent on storm characteristics, antecedent catchment wetness conditions, landscape properties and catchment size (Fischer et al., 2017; von Freyberg et al., 2018). However, separating groundwater and soil water with stable isotopes alone can be problematic. Stable isotope composition may not differ enough between soil water and groundwater or show a high variation in space and time (Klaus and McDonnell, 2013). Consequently, other environmental tracers have been utilized to characterize hydrologic flow paths. Water stable isotopes have, e.g., been coupled with hydrochemistry to disentangle contribution from the unsaturated and saturated zone (Ladouche et al., 2001). Furthermore, radon has proven to be useful in this context. Genereux et al. (1993) used the different ^{222}Rn signatures of vadose zone water, soil water, and bedrock groundwater in a three end-member mixing model and showed groundwater and soil water to be the dominant sources of streamflow during low-flow periods. Kies et al. (2005) showed with ^{222}Rn data during a high-flow event the timing of groundwater pushing into the stream. Kienzler and Naef (2008) used ^{222}Rn in an experiment with added artificial tracers revealing that soil water is rapidly released from saturated patches and explains high contribution of pre-event water in the storm hydrograph. Webb et al. (2017) and Liao et al. (2021) used ^{222}Rn to show the dynamic contribution of groundwater to a floodplain and highlighted the importance to capture floods appropriately to avoid their underestimation.

With the availability of continuous measurements of ^{222}Rn using mobile equipment, this tracer fed into the suite of chemical and isotopic high-frequency measurements available for surface waters to improve understanding of subsurface stormflow (Chifflard et al., 2019) and timing of groundwater input (Unland et al., 2013). However, as with any dissolved gas tracer (and as discussed in Section 2.2.2) gas transfer

velocities need to be thoroughly determined. Even though it was shown that these can be well determined even in high gradient streams (Gleeson et al., 2018), high-flow events certainly add complexity. The resulting increased turbulence with higher flow velocity, debris or clogging, and precipitation falling on the stream would require continuous monitoring of gas transfer velocity (Klaus et al., 2019). Another uncertainty arises from draining of aquifers with different ^{226}Ra content, i.e., a spatially varying ^{222}Rn endmember. Here the combination with other geogenic tracers such as hydrochemistry or stable isotopes of strontium (Hogan and Blum, 2003), sulphate (Gu et al., 2008) or carbonate (Meredith and Kuzara, 2012) could be useful.

Beyond understanding the hydrology of catchments, the residence time distribution of the groundwater also impacts water quality at the catchment scale (Van der Velde et al., 2010; Pinay et al., 2015; Raymond et al., 2016; Barnes et al., 2018; Hare et al., 2021). The inclusion of radioisotopes into hydrological modelling was particularly useful to understand the "old water paradox", describing the rapid mobilization of "old" water in traditional hydrograph separation studies (Stewart et al., 2010). Particularly seasonal tracers such as stable water isotopes didn't represent the long tails of travel-time distributions. ^{3}H has often been used to study the mean age of streamflow (Duvert et al., 2016; Cartwright and Morgenstern, 2018), however, tracers with a shorter half-life should be added, as rivers compose of a large fraction of sub-yearly water age (Jasechko et al., 2016). While one could argue that these fractions are covered by seasonal tracers (Kirchner, 2016), short-lived radioisotopes have the potential to prove/disprove the young water fraction calculated based on seasonal tracers.

Kaste et al. (2016) suggested that the 2.6-year half-life makes ^{22}Na a perfect tracer for the 1–20 years characteristic timescale of many catchment-scale transport processes. Visser et al. (2019) used stable water isotopes, ^{3}H, ^{22}Na, and ^{35}S to determine water ages of streamflow for a catchment in the Sierra Nevada. The unique combination of these age tracers allowed them to constrain the parameters of a hydrological model and determine the relationship between the ages of water that is stored in the catchment and water in the stream. However, studies on ^{22}Na, and ^{35}S are restricted at the moment to very small headwater streams in the litre per second range. ^{35}S, covering very well the young water fraction with regards to its half-life, has the potential to quantify accurately the proportion of event water.

It can be concluded that only a combination of tracers reaches to an accurate approximation of the hydrochronology of a stream. As stream water is mainly composed of shallow groundwater (Ferguson et al., 2023), the use of short-lived radioisotopes to refine hydrological models seems only logical. "Super-sites", i.e., well-equipped exemplary catchments, that allow testing different tracers and process-based hydrological models could be a promising way forward to improve our understanding of streamflow generation under a changing climate.

3.5. *Precipitation characteristics and groundwater recharge mechanisms – an outlook*

Isotope hydrology is using stable isotopes to understand factors such as the minimum precipitation rate to achieve groundwater recharge or tracing single recharge events through highly dynamic systems, i.e., isotope tempestology (e.g., Welsh and Sánchez-Murillo, 2020). Radiogenic isotopes vary similarly in their activity concentrations with the different precipitation events (see Sections 2.1.1. and 2.1.5). Precipitation type (snow/rain, drop size, intensity), origin of air masses, cloud formation and seasonality influence the activity concentration (Ioannidou and Papastefanou, 2006; Schubert et al., 2021; Terzer-Wassmuth et al., 2022a, 2022b). Therefore, short-lived cosmogenic radionuclides have the potential to complement water stable isotopes and ^{3}H to enhance understanding of different precipitation events and their impact on water resources. However, we are not aware of any studies so far that were using multi-tracer approaches including water stable isotopes, ^{3}H and short-lived radionuclides for investigating the impact of specific precipitation events on groundwater recharge. Further investigation is encouraged here.

4. Conclusions

- Many tracers presented in this review have either not yet been applied in hydrogeological studies at all (^{32}P/^{33}P) or have been used for this purpose only very sparsely (^{35}S, ^{7}Be). $^{224/223}$Ra has been used widely as aqueous tracer, but only in very specific applications mainly in the coastal sea. ^{222}Rn has been used in a wide range of groundwater/surface water interaction studies. Still, its half-life would also allow using it to narrow down estimated ages deduced from ^{35}S or ^{7}Be data (for example in studies looking at river bank infiltration or at MAR sites). Similarly, cosmogenic isotopes could help to reduce uncertainties that are related to unknown ^{222}Rn degassing rates in open channels or emanation rates of ^{222}Rn. Hence, the full potential of multi-tracer approaches using short-lived radioisotopes is only insufficiently exploited yet and needs to be assessed more thoroughly.
- For water resource managers, the short-lived, naturally occurring radioisotopes presented in this review have clear advantages over artificial tracer tests or pumping tests. These advantages include reliable minimum residence times without the need to monitor the spring or well continuously and the assessment of dynamic systems over time such as river banks, flood plains and MAR sites. To have reliable information that the youngest water fraction in a system is not below a year is in many assessments most important, as it allows to assess vulnerability to pathogens, contamination from industrial accidents and natural disasters.
- One way to accelerate the application and to use the benefits of multi-tracer approaches applying short-lived radioisotopes would be to test their joint utilisation and compare their individual suitability at well-equipped "super-sites" characterized by exemplary and well-known hydrogeological settings. Some of the discussed tracers have already been tested in such model catchments or well fields but to our knowledge there is no study that combined thorough monitoring of any of the presented short-lived isotopes over at least one year in precipitation and/or surface water or groundwater. Furthermore, most field studies were not combined with complementary experiments such as tracer retention in the soil or aquifer matrix or impact of different rock/sediment types.
- Besides the benefits for hydrogeological studies, monitoring the suite of cosmogenic radioisotopes at such a "super-site" in precipitation would also improve our understanding of cosmogenic ^{3}H in the atmosphere. Consequently, this would improve the attempts to model ^{3}H in the atmosphere and its use as an age tracer in hydrogeology.

Additionally, to the "super-site" approach, global data is needed to verify the applicability of cosmogenic radioisotopes as proxy parameters for each other. For precipitation ^{35}S there was no data found for the tropics and the southern Hemisphere; for radio-phosphorus only two studies exist. Even though ^{7}Be is much better investigated there is still little comparative studies to investigate the differences between air and precipitation samplers.

CRediT authorship contribution statement

Michael Schubert: Writing – review & editing, Writing – original draft, Conceptualization. **Mang Lin:** Writing – review & editing, Conceptualization. **Jordan F. Clark:** Writing – review & editing. **Martin Kralik:** Writing – review & editing. **Sandra Damatto:** Writing – review & editing. **Lorenzo Copia:** Writing – review & editing. **Stefan Terzer-Wassmuth:** Writing – review & editing. **Astrid Harjung:** Writing – review & editing, Supervision, Conceptualization.

Declaration of competing interest

The authors declare that they have no known competing financial interests or personal relationships that could have appeared to influence the work reported in this paper.

Data availability

Data will be made available on request.

Acknowledgements

The review paper was initiated by an IAEA Technical Meeting on "Application of Short-Lived Radionuclides for Surface Water and Shallow Groundwater Vulnerability Assessment" (EVT2205126), held virtually on 6–10 February 2023. M.L. was supported by the National Natural Science Foundation of China (42325301) and CIFAR Azrieli Global Scholars Program. Funding was provided to JFC from the Water Reuse Research Foundation (WRRF-09-11) in cooperation with the Water Replenishment District of Southern California, the Orange County Water District, the State of California Groundwater Ambient Monitoring and Assessment (GAMA) Special Studies Program, and the Lawrence Graduate Scholarship Program at the Lawrence Livermore National Laboratory. Data from the Oulu Neutron Monitor was obtained from the Sodankylä Geophysical Observatory (https://cosmicrays.oulu.fi/). The studies in the Austrian Alps were funded by the Environment Agency Austria and the Vorarlberger Landesregierung.

References

Abbott, B.W., Baranov, V., Mendoza-Lera, C., et al., 2016. Using multi-tracer inference to move beyond single-catchment ecohydrology. Earth Sci. Rev. 160, 19–42.

Adyasari, D., Dimova, N.T., Dulai, H., Gilfedder, B.S., Cartwright, I., McKenzie, T., Fuleky, P., 2023. Radon-222 as a groundwater discharge tracer to surface waters. Earth Sci. Rev. 104321.

Akata, N., Kakiuchi, H., Shima, N., Iyogi, T., Momoshima, N., Hisamatsu, S.I., 2011. Tritium concentrations in the atmospheric environment at Rokkasho, Japan before the final testing of the spent nuclear fuel reprocessing plant. J. Environ. Radioact. 102 (9), 837–842.

Andrews, J.N., Wood, D.F., 1972. Mechanism of radon release in rock matrices and entry into groundwaters. Trans. Inst. Min. Metall. A Min. Technol. B81, 198–209.

Atkinson, A.P., Cartwirght, I., Gilfedder, B.S., Hofmann, H., Unland, N.P., Cendón, D.I., Chisari, R., 2013. A multi-tracer approach to quantifying groundwater inflows to an upland river; assessing the influence of variable groundwater chemistry. Hydrol. Process. 29 (1), 1–12. https://doi.org/10.1002/hyp.10122.

Bansah, S., Ali, G., 2017. Evaluating the effects of tracer choice and end-member definitions on hydrograph separation results across nested, seasonally cold watersheds. Water Resour. Res. 53, 8851–8871. https://doi.org/10.1002/2016WR020252.

Barbulescu, A., 2020. Assessing groundwater vulnerability: DRASTIC and DRASTIC-like methods: a review. Water 12 (5), 1356.

Barnes, R.T., Butman, D.E., Wilson, H.F., Raymond, P.A., 2018. Riverine export of aged carbon driven by flow path depth and residence time. Environ. Sci. Technol. 52 (3), 1028–1035.

Barthold, F.K., Tyralla, C., Schneider, K., Vaché, K.B., Frede, H.-G., Breuer, L., 2011. How many tracers do we need for end member mixing analysis (EMMA)? A sensitivity analysis. Water Resour. Res. 47, W08519 https://doi.org/10.1029/2011WR010604.

Beck, A.J., Cochran, M.A., 2013. Controls on solid-solution partitioning of radium in saturated marine sands. Mar. Chem. 156, 38–48. https://doi.org/10.1016/j.marchem.2013.01.008.

Benitez-Nelson, C.R., Buesseler, K.O., 1998. Measurement of cosmogenic ^{32}P and ^{33}P activities in rainwater and seawater. Anal. Chem. 70 (1), 64–72. https://doi.org/10.1021/ac9707500.

Bhandari, N., Lal, D., Rama, 1970. Vertical structure of the troposphere as revealed by radioactive tracer studies. J. Geophys. Res. 75, 2974–2980.

Black, G., Sharpless, R.L., Slanger, T.G., 1982. Rate coefficients at 298 K for SO reactions with O_2, O_3, and NO_2. Chem. Phys. Lett. 90, 55–58.

Bond, M.J., Carr, J., 2018. Permafrost thaw and implications for the fate and transport of tritium in the Canadian north. J. Environ. Radioact. 192, 295–311.

Brothers, L.A., Dominguez, G., Abramian, A., Corbin, A., Bluen, B., Thiemens, M.H., 2010. Optimized low-level liquid scintillation spectroscopy of S^{-35} for atmospheric and biogeochemical chemistry applications. P. Natl. Acad. Sci. USA 107, 5311–5316.

Burnett, W.C., Dulaiova, H., 2003. Estimating the dynamics of groundwater input into the coastal zone via continuous radon-222 measurements. J. Environ. Radioact. 69, 21–35.

Burnett, W.C., Taniguchi, M., Oberdorfer, J., 2001. Measurement and significance of the direct discharge of groundwater into the coastal zone. J. Sea Res. 46 (2), 109–116. https://doi.org/10.1016/S1385-1101(01)00075-2.

Burnett, W.C., et al., 2006. Quantifying submarine groundwater discharge in the coastal zone via multiple methods. Sci. Total Environ. 367 (2–3), 498–543. https://doi.org/10.1016/j.scitotenv.2006.05.009.

Burnett, W.C., Peterson, R., Moore, W.S., de Oliveira, J., 2008. Radon and radium isotopes as tracers of submarine groundwater discharge – results from the Ubatuba, Brazil SGD assessment intercomparison. Estuar. Coast. Shelf Sci. 76 (3), 501–511. https://doi.org/10.1016/j.ecss.2007.07.027.

Burnett, W.C., Wattayakorn, G., Supcharoen, R., Sioudom, K., Kum, V., Chanyotha, S., Kritsananuwat, R., 2017. Groundwater discharge and phosphorus dynamics in a flood-pulse system: Tonle Sap Lake, Cambodia. J. Hydrol. 549, 79–91. https://doi.org/10.1016/j.jhydrol.2017.03.049.

Burns, D.A., Murdoch, P.S., Lawrence, G.B., Michel, R.L., 1998. Effect of groundwater springs on NO_3- concentrations during summer in Catskill Mountain streams. Water Resour. Res. 34 (8), 1987–1996. https://doi.org/10.1029/98WR01282.

Cable, J.E., Martin, J.B., 2008. In situ evaluation of nearshore marine and fresh pore water transport into Flamengo Bay, Brazil. Estuar. Coast. Shelf Sci. 76 (3), 473–483. https://doi.org/10.1016/j.ecss.2007.07.045.

Cable, J.E., Burnett, W.C., Chanton, J.P., Weatherly, G., 1996. Modelling groundwater flow into the ocean based on 222Rn. Earth Planet. Sci. Lett. 144, 591–604.

Cantaloub, M., Higginbotham, J., Semprini, L., 1997. The determination of Rn partition coefficients for several liquid scintillation cocktails. In: Proceedings, 43rd Annual Conference on Bioassay, Analytical and Environmental Radiochemistry, Charleston S.C.

Carlyle, G.C., Hill, A.R., 2001. Groundwater phosphate dynamics in a river riparian zone: effects of hydrologic flow paths, lithology and redox chemistry. J. Hydrol. 247, 151–168. https://doi.org/10.1016/S0022-1694(01)00375-4.

Cartwright, I., Gilfedder, B.S., 2015. Mapping and quantifying groundwater inflows to Deep Creek (Maribyrnong catchment, SE Australia) using 222Rn, implications for protecting groundwater-dependant ecosystems. Appl. Geochem. 52, 118–129.

Cartwright, I., Morgenstern, U., 2018. Using tritium and other geochemical tracers to address the "old water paradox" in headwater catchments. J. Hydrol. 563, 13–21. https://doi.org/10.1016/j.jhydrol.2018.05.060.

Cauquoin, A., Jean-Baptiste, P., Risi, C., Fourré, É., Stenni, B., Landais, A., 2015. The global distribution of natural tritium in precipitation simulated with an Atmospheric General Circulation Model and comparison with observations. Earth Planet. Sci. Lett. 427, 160–170.

Chae, J.S., Kim, G., 2019. Seasonal and spatial variations of tritium in precipitation in Northeast Asia (Korea) over the last 20 years. J. Hydrol. 574, 794–800.

Chen, T.-C., Shih, Y.-J., Chang, C.C., Huang, Y.-H., 2013. Novel adsorbent of removal phosphate from TFT LCD wastewater. J. Taiwan Inst. Chem. Eng. 44 (1), 61–66.

Chifflard, P., et al., 2019. How can we model subsurface stormflow at the catchment scale if we cannot measure it? Hydrol. Process. 33 (9), 1378–1385. https://doi.org/10.1002/hyp.13407.

Cho, H.-M., Hong, Y.-L., Kim, G., 2011. Atmospheric deposition fluxes of cosmogenic ^{35}S and ^{7}Be: implications for the turnover rate of sulfur through the biosphere. Atmos. Environ. 45, 4230–4234.

Christensen, T.H., Kjeldsen, P., Bjerg, P.L., Jensen, D.L., Christensen, J.B., Baum, A., Jørgen, H.-J., Heron, G., 2001. Biogeochemistry of landfill leachate plumes. J. Appl. Geochem. 16, 659–718.

Clark, J.F., Hudson, G.B., Davisson, M.L., Woodside, G., Herndon, R., 2004. Geochemical imaging of flow near an artificial recharge facility, Orange County, CA. Ground Water 42, 167–174.

Clark, J.F., Morrissey, S., Dadakis, J., Hutchinson, A., Herndon, R., 2014. Investigation of groundwater flow variations near a spreading pond with repeat deliberate tracer experiments. Water 6, 1826–1839.

Clark, J.F., Uriostegui, S.H., Bibby, R.K., Esser, B.K., Tredoux, G., 2016. Quantifying apparent groundwater ages near managed aquifer recharge operations using ^{35}S as an intrinsic tracer. Water 8. https://doi.org/10.3390/W6061826.

Cook, P.G., Herczeg, A.L., 2000. Environmental Tracers in Subsurface Hydrology. Kluwer Academic Press, Dordrecht, Netherlands.

Cook, P.G., Lamontagne, S., Berhane, D., Clark, J.F., 2006. Quantifying groundwater discharge to Cockburn River, southeastern Australia, using dissolved gas tracers ^{222}Rn and SF_6. Water Resour. Res. 42 (10), 1–12.

Cook, P.G., Rodellas, V., Andrisoa, A., Stieglitz, T.C., 2018. Exchange across the sediment-water interface quantified from porewater radon profiles. J. Hydrol. 559, 873–883.

Cooper, L.W., Olsen, C.R., Solomon, D.K., Larsen, I.L., Cook, R.B., Grebmeier, J.M., 1991. Stable isotopes of oxygen and natural and fallout radionuclides used for tracing runoff during snowmelt in an artic watershed. Water Resour. Res. 27, 2171–2179.

Corbett, D.R., Burnett, W.C., Cable, P.H., Clark, S.B., 1998. A multiple approach to the determination of radon fluxes from sediments. J. Radioanal. Nucl. Chem. 236 (1–2), 247–252.

Corcho-Alvarado, J., Pačes, T., Purtschert, R., 2013. Dating groundwater in the Bohemian Cretaceous Basin: understanding tracer variations in the subsurface. J. Appl. Geochem. 29, 189–198.

Correll, D.L., 1998. The role of phosphorus in the eutrophication of receiving waters: a review. J. Environ. Qual. 27, 261–266. https://doi.org/10.2134/jeq1998.00472425002700020004x.

Courtier, J., Sdraulig, S., Hirth, G., 2017. 7Be and 210Pb wet/dry deposition in Melbourne, Australia and the development of deployable units for radiological emergency monitoring. J. Environ. Radioact. 178–179, 419–425. https://doi.org/10.1016/j.jenvrad.2017.07.004.

Cristofanelli, A., Bracci, A., Sprenger, M., Marinoni, A., Bonafe, U., Calzolari, F., Duchi, R., Laj, P., Pichon, J.M., Roccato, F., Venzac, H., Vuillermoz, E., Bonasoni, P., 2010. Tropospheric ozone variations at the Nepal Climate Observatory-Pyramid (Himalayas, 5079m asl) and influence of deep stratospheric intrusion events. Atmos. Chem. Phys. 10, 6537–6549.

Deinhart, A.L., Bibby, R.K., Visser, A., Thaw, M., Thomas, K., 2021. Simplified method for the in situ collection and laboratory analysis of cosmogenic tracers (Sulfur-35 and Sodium-22) to determine residence time distributions and water ages. Anal. Chem. 93 (10), 4472–4478. https://doi.org/10.1021/acs.analchem.0c04490.

Del Campillo, M.C., van der Zee, S.E.A.T.M., Torrent, J., 1999. Modelling long-term phosphorus leaching and changes in phosphorus fertility in excessively fertilized acid sandy soils. Eur. J. Soil Sci. 50, 391–399.

Delaygue, G., Bekki, S., Bard, E., 2015. Modelling the stratospheric budget of beryllium isotopes. Tellus B 67 (28582), 2015. https://doi.org/10.3402/tellusb.v67.28582.

Di Stefano, E., Baccolo, G., Clemenza, M., Delmonte, B., Fiorini, D., Garzonio, R., Schwikowski, M., Maggi, V., 2023. Evidence of radionuclide fractionation due to meltwater percolation in a temperate glacier. Cryosphere Discuss. 1–17.

Diego-Feliu, M., Rodellas, V., Alorda-Kleinglass, A., Tamborski, J., van Beek, P., Heins, L., Bruach-Menchén, J.M., Arnold, R., Garcia-Orellana, J., 2020. Guidelines and limits for the quantification of Ra isotopes and related radionuclides with the Radium Delayed Coincidence Counter (RaDeCC). J. Geophys. Res. C Ocean 125. https://doi.org/10.1029/2019JC015544.

Diego-Feliu, M., Rodellas, V., Saaltink, M.W., Alorda-Kleinglass, A., Goyetche, T., Martínez-Pérez, L., Folch, A., Garcia-Orellana, J., 2021. New perspectives on the use of 224Ra/228Ra and 222Rn/226Ra activity ratios in groundwater studies. J. Hydrol. 596, 126043 https://doi.org/10.1016/j.jhydrol.2021.126043.

Dimova, N., Burnett, W.C., 2011. Evaluation of groundwater discharge into small lakes based on the temporal distribution of Rn-222. Limnol. Oceanogr. 56 (2), 486–494. https://doi.org/10.4319/lo.2011.56.2.0486.

Dimova, N.T., Burnett, W.C., Chanton, J.P., Corbett, J.E., 2013. Application of radon-222 to investigate groundwater discharge into small shallow lakes. J. Hydrol. 486, 112–122. https://doi.org/10.1016/j.jhydrol.2013.01.043.

Doering, Ch., Saey, P., 2013. Hadley cell influence on Be-7 activity concentrations at Australian mainland IMS radionuclide particulate stations. J. Environ. Radioact. 127C, 88–94. https://doi.org/10.1016/j.jenvrad.2013.10.011.

Duliński, M., Różański, K., Pierchała, A., Gorczyca, Z., Marzec, M., 2019. Isotopic composition of precipitation in Poland: a 44-year record. Acta Geophys. 67, 1637–1648.

Duvert, C., Stewart, M.K., Cendón, D.I., Raiber, M., 2016. Time series of tritium, stable isotopes and chloride reveal short-term variations in groundwater contribution to a stream. Hydrol. Earth Syst. Sci. 20 (1), 257–277.

Eastoe, C.J., Watts, C.J., Ploughe, M., Wright, W.E., 2012. Future use of tritium in mapping pre-bomb groundwater volumes. Groundwater 50 (1), 87–93.

Ehhalt, D.H., Rohrer, F., Schauffler, S., Pollock, W., 2002. Tritiated water vapor in the stratosphere: vertical profiles and residence time. J. Geophys. Res.-Atmos. 107 (D24), ACH-8.

Ekwurzel, B., Schlosser, P., Smethie Jr., W.M., Plummer, L.N., Busenberg, E., Michel, R. L., Weppering, R., Stute, M., 1994. Dating of shallow groundwater: comparison of the transient tracers $^{3}H/^{3}He$, chlorofluorocarbons, and ^{85}Kr. Water Resour. Res. 30 (6), 1693–1708.

Elsinger, R.J., Moore, W.S., 1983. 224Ra,228Ra, and226Ra in Winyah Bay and Delaware Bay. Earth Planet. Sci. Lett. 64 (3), 430–436. https://doi.org/10.1016/0012-821X(83)90103-6.

Feldman, U., Schühle, U., Widing, K.G., Laming, J.M., 1998. Coronal composition above the solar equator and the north pole as determined from spectra acquired by the SUMER instrument on SOHO. Astrophys. J. 505, 999–1006.

Ferguson, G., McIntosh, J.C., Jasechko, S., 2023. Groundwater deeper than 500 m contributes less than 0.1% of global river discharge. Commun. Earth. Environ. 4, 48. https://doi.org/10.1038/s43247-023-00697-6.

Fifield, L.K., Morgenstern, U., 2009. Silicon-32 as a tool for dating the recent past. Quat. Geochronol. 4, 400–405.

Firestone, R.B., Shirley, V.S., Baglin, C.M., Frank Chu, S.Y., Zipkin, J., 1996. Table of Isotopes, , 8th ed.Vol. I. John Wiley & Sons, Inc, Hoboken.

Fischer, B.M.C., Stähli, M., Seibert, J., 2017. Pre-event water contributions to runoff events of different magnitude in pre-alpine headwaters. Hydrol. Res. 48, 28–47. https://doi.org/10.2166/nh.2016.176.

Fourré, E., Jean-Baptiste, P., Dapoigny, A., Baumier, D., Petit, J.R., Jouzel, J., 2006. Past and recent tritium levels in Arctic and Antarctic polar caps. Earth Planet. Sci. Lett. 245 (1–2), 56–64.

Fourré, E., Landais, A., Cauquoin, A., Jean-Baptiste, P., Lipenkov, V., Petit, J.R., 2018. Tritium records to trace stratospheric moisture inputs in Antarctica. J. Geophys. Res.-Atmos. 123 (6), 3009–3018.

Frei, S., Gilfedder, B.S., 2015. Technical note: FINIFLUX an implicit finite element model for quantification of groundwater fluxes and hyporheic exchange in streams and rivers using Radon. Water Resour. Res. 51, 6776–6786.

Frei, S., Durejka, S., Le Lay, H., Thomas, Z., Gilfedder, B.S., 2019. Quantification of hyporheic nitrate removal at the reach scale: exposure times versus residence times. Water Resour. Res. 55, 9808–9825.

Frei, S., Wismeth, F., Gilfedder, B.S., 2020. Quantifizierung lokaler Grundwassereintritte in die Spree und deren Bedeutung für die Verockerungsproblematik in der Lausitz. Grundwasser - Zeitschrift der Fachsektion Hydrogeologie 25 (3), 231–241.

Frey, S., Kuells, C., Schlosser, C., 2011. New Hydrological Age-dating Techniques Using Cosmogenic Radionuclides Beryllium-7 and Sodium-22 (No. IAEA-CN-186). IAEA-CN-186.

Freyer, K., Treutler, H.C., Dehnert, J., Nestler, N., 1997. Sampling and measurement of radon-222 in water. J. Environ. Radioact. 37 (3), 327–337. https://doi.org/10.1016/S0265-931X(96)00102-6.

Galvin, A.B., et al., 1996. Solar wind composition: first results from SOHO and future expectations. Bull. Am. Astron. Soc. 28, 897.

Garcia-Orellana, J., Rodellas, V., Tamborski, J., Diego-Feliu, M., van Beek, P., Weinstein, Y., Charette, M., Alorda-Kleinglass, A., Michael, H.A., Stieglitz, T., Scholten, J., 2021. Radium isotopes as submarine groundwater discharge (SGD) tracers: review and recommendations. Earth Sci. Rev. 103681.

Genereux, D.P., Hemond, H.F., Mulholland, P.J., 1993. Use of radon-222 and calcium as tracers in a three-end-member mixing model for streamflow generation on the West Fork of Walker Branch Watershed. J. Hydrol. 142, 167–211. https://doi.org/10.1016/0022-1694(93)90010-7.

Gibson, J.J., Birks, S.J., Yi, Y., 2016. Higher tritium concentrations measured in permafrost thaw lakes in northern Alberta. Hydrol. Process. 30 (2), 245–249.

Giffin, C., Kaufman, A., Broecker, W., 1963. Delayed coincidence counter for the assay of actinon and thoron. J. Geophys. Res. 68 (6), 1749–1757. https://doi.org/10.1029/JZ068i006p01749.

Gill, R.C.O., 1993. Geochemische Grundlagen der Geowissenschaften. Enke, Stuttgart/Deutschland.

Gleeson, T., Manning, A.H., Popp, A., Zane, M., Clark, J.F., 2018. The suitability of using dissolved gases to determine groundwater discharge to high gradient streams. J. Hydrol. 557, 561–572.

Gray, C.W., Pang, L., Dodd, R., McDowell, R.W., Close, M.E., 2015. Transport of phosphorus in an alluvial gravel aquifer. New Zealand J. Agric. 58 (4), 490–501. https://doi.org/10.1080/00288233.2015.1080737.

Grunbaum, Z., Kroll, K., Greene, J.L., Rasey, J.S., Krohn, K.A., 1990. Synthesis and radiobiological applications of [35S]l-homocysteine thiolactone. International Journal of Radiation Applications and Instrumentation. Part B. Nucl. Med. Biol. 17 (5), 473–478. https://doi.org/10.1016/0883-2897(90)90166-X.

Gu, A., Gray, F., Eastoe, C.J., Norman, L.M., Duarte, O., Long, A., 2008. Tracing ground water input to base flow using sulfate (S, O) isotopes. Groundwater 46, 502–509. https://doi.org/10.1111/j.1745-6584.2008.00437.x.

Guo, F., Guanghui, J., Fan, L., 2021. Biological sulfate reduction in an epigene karst aquifer and its impact on cave environment. J. Hydrol. 602, 126804.

Hancock, G.J., Webster, I.T., Stieglitz, T.C., 2006. Horizontal mixing of great barrier reef water: offshore diffusivity determined from radium isotope distributions. J. Geophys. Res. 111, C12019 https://doi.org/10.1029/2006JC003608.

Hare, D.K., Helton, A.M., Johnson, Z.C., Lane, J.W., Briggs, M.A., 2021. Continental-scale analysis of shallow and deep groundwater contributions to streams. Nat. Commun. 12, 1450. https://doi.org/10.1038/s41467-021-21651-0.

Harjung, A., Schweichhart, J., Rasch, G., Griebler, C., 2023. Large-scale study on groundwater dissolved organic matter reveals a strong heterogeneity and a complex microbial footprint. Sci. Total Environ. 854, 158542.

Harms, P.A., Visser, A., Moran, J.E., Esser, B.K., 2016. Distribution of tritium in precipitation and surface water in California. J. Hydrol. 534, 63–72.

Harris, S.H., Istok, J.D., Suflita, J.M., 2006. Changes in organic matter biodegradability influencing sulfate reduction in an aquifer contaminated by landfill leachate. Microb. Ecol. 51, 535–542.

Hartmann, A., Jasechko, S., Gleeson, T., Wada, Y., Andreo, B., Barberá, J.A., et al., 2021. Risk of groundwater contamination widely underestimated because of fast flow into aquifers. Proc. Natl. Acad. Sci. U. S. A. 118 (20), e2024492118.

Hebert, D., 2011. Tritium in precipitation of Vostok (Antarctica): conclusions on the tritium latitude effect. Isot. Environ. Health Stud. 47 (3), 265–272.

Hernández-Ceballos, M.A., Marín Ferrer, M., Cinelli, G., Tollefsen, T., De Felice, L., Nweke, E., et al., 2015. A climatology of 7Be in surface air in European Union. J. Environ. Radioact. 141, 62–70.

Hiyama, T., Dashtseren, A., Asai, K., Kanamori, H., Iijima, Y., Ishikawa, M., 2021. Groundwater age of spring discharges under changing permafrost conditions: the Khangai Mountains in Central Mongolia. Environ. Res. Lett. 16 (1), 015008.

Hofmann, H., Gilfedder, B.S., Cartwright, I., 2011. A novel method using a silicone diffusion membrane for continuous ^{222}Rn measurements for the quantification of groundwater discharge to streams and rivers. Environ. Sci. Technol. 45 (20), 8915–8921.

Hogan, J.F., Blum, J.D., 2003. Tracing hydrologic flow paths in a small forested watershed using variations in (87)Sr, (86)Sr,[Ca]/[Sr], [Ba]/[Sr] and Delta O-18. Water Resour. Res. 39 (10) https://doi.org/10.1029/2002WR001856.

Hohwieler, N., 2005. Beryllium-7 als neuer Tracer in der hydrologischen Prozessforschung - eine Machbarkeitsstudie, Masters Thesis. Institut fuer Hydrologie der Universitaet Freiburg.

Hong, Y., Kim, G., 2005. Measurement of cosmogenic ^{35}S activity in rainwater and lake water. Anal. Chem. 77, 3390–3393.

IAEA, 2014. Guidelines for Using Fallout Radionuclides to Assess Erosion and Effectiveness of Soil Conservation Strategies (No. IAEA-TECDOC-1741). Joint FAO/IAEA Division of Nuclear Techniques in Food and Agriculture.

IAEA/WMO, 2023. Global Network of Isotopes in Precipitation. The GNIP Database. https://nucleus.iaea.org/wiser. (Accessed 20 September 2023).

Ioannidou, A., Papastefanou, C., 2006. Precipitation scavenging of ^{7}Be and ^{137}Cs radionuclides in air. J. Environ. Radioact. 85 (1), 121–136.

Iurian, A.R., Toloza, A., Adu-Gyamfi, J., Cosma, C., 2013. Spatial distribution of ^{7}Be in soils of Lower Austria after heavy rains. J. Radioanal. Nucl. Chem. 298, 1857–1863. https://doi.org/10.1007/s10967-013-2683-8.

Ivanovich, M., Harmon, R.S., 1992. Uranium-Series Disequilibrium, 2nd ed. Clarendon Press, Oxford.

Jasechko, S., Kirchner, J.W., Welker, J.M., McDonnell, J.J., 2016. Substantial proportion of global streamflow less than three months old. Nat. Geosci. 9 (2), 126–129.

Jefanova, O., Mažeika, J., Petrošius, R., Skuratovič, Ž., 2018. The distribution of tritium in aquatic environments. Lithuania. J. Environ. Radioact. 188, 11–17.
Juhlke, T.R., Sültenfuß, J., Trachte, K., Huneau, F., Garel, E., Santoni, S., et al., 2020. Tritium as a hydrological tracer in Mediterranean precipitation events. Atmos. Chem. Phys. 20 (6), 3555–3568.
Jurgens, B.C., Faulkner, K., McMahon, P.B., Hunt, A.G., Casile, G., Young, M.B., Belitz, K., 2022. Over a third of groundwater in USA public-supply aquifers is Anthropocene-age and susceptible to surface contamination. Nat. Commun. Earth Environ. 3 (1), 153. https://doi.org/10.1038/s43247-022-00473-y.
Kaste, J.M., Norton, S.A., Hess, C.T., 2002. Environmental chemistry of beryllium-7. Rev. Mineral. Geochem. 50 (1), 271–289.
Kaste, J.M., Lauer, N.E., Spaetzel, A.B., Goydan, C., 2016. Cosmogenic 22Na as a steady-state tracer of solute transport and water age in first-order catchments. Earth Planet. Sci. Lett. 456, 78–86. https://doi.org/10.1016/j.epsl.2016.10.002.
Kester, C., Baron, J., Turk, J., 2003. Isotopic study of sulfate sources and residence times in a subalpine watershed. Environ. Geol. 43, 606–613.
Keulegan, G.H., 1967. Tidal Flow in Entrances. U.S. Army Corps of Engineers, Committee on Tidal Hydraulics, Tech. Bull, p. 14.
Kienzler, P.M., Naef, F., 2008. Subsurface storm flow formation at different hillslopes and implications for the 'old water paradox'. Hydrol. Process. 22, 104–116. https://doi.org/10.1002/hyp.6687.
Kies, A., Hofmann, H., Tosheva, Z., Hoffmann, L., Pfister, L., 2005. Using ^{222}Rn for hydrograph separation in a micro basin (Luxembourg). Ann. Geophys. 48 https://doi.org/10.4401/ag-3184.
Kirchner, J.W., 2016. Aggregation in environmental systems – part 1: seasonal tracer cycles quantify young water fractions, but not mean transit times, in spatially heterogeneous catchments. Hydrol. Earth Syst. Sci. 20, 279–297. https://doi.org/10.5194/hess-20-279-2016.
Klaus, J., McDonnell, J.J., 2013. Hydrograph separation using stable isotopes: review and evaluation. J. Hydrol. 505, 47–64. https://doi.org/10.1016/j.jhydrol.2013.09.006.
Klaus, M., Geibrink, E., Hotchkiss, Erin R., Karlsson, J., 2019. Listening to air–water gas exchange in running waters. Limnol. Oceanogr. Methods 17 (7), 395–414. https://doi.org/10.1002/lom3.10321.
Klaus, M., Labasque, T., Botter, G., Durighetto, N., Schelker, J., 2022. Unravelling the contribution of turbulence and bubbles to air-water gas exchange in running waters. Eur. J. Vasc. Endovasc. Surg. 127, e2021JG006520 https://doi.org/10.1029/2021JG006520.
Kluge, T., Ilmberger, J., von Rohden, C., Aeschbach-Hertig, W., 2007. Tracing and quantifying groundwater inflow into lakes using a simple method for radon-222 analysis. Hydrol. Earth Syst. Sci. 11, 1621–1631.
Knöller, K., Schubert, M., 2010. Interaction of dissolved and sedimentary sulfur compounds in contaminated aquifers. Chem. Geol. 276, 284–293.
Knöller, K., Trettin, R., Strauch, G., 2005. Sulphur cycling in the drinking water catchment area of Torgau-Mockritz (Germany); insights from hydrochemical and stable investigations. Hydrol. Process. 19, 3445–3465.
Knöller, K., Vogt, C., Feisthauser, S., Weise, S.M., Weiss, H., Richnow, H.H., 2008. Sulfur cycling and biodegradation in contaminated aquifers: insights from stable isotope investigations. Environ. Sci. Technol. 42, 7807–7812.
Koch, D., Rind, D., 1998. ^{10}Be/^{7}Be as a tracer for atmospheric transport. J. Geophys. Res. 103, 3907–3917.
Koch, D.M., Jacob, D.J., Graustein, W.C., 1996. Vertical transport of tropospheric aerosols as indicated by ^{7}Be and ^{210}Pb in chemical tracer model. J. Geophys. Res. 101 (D13), 18651–18666.
Köllő, Z., Palcsu, L., Major, Z., Papp, L., Molnár, M., Ranga, T., et al., 2011. Experimental investigation and modelling of tritium washout by precipitation in the area of the nuclear power plant of Paks. Hungary. J. Environ. Radioact. 102 (1), 53–59.
Kralik, M., 2015. How to estimate mean residence times of groundwater. Procedia Earth Planet. Sci. 13, 301–306.
Kralik, M., Vergnaud, V., Uriostegui, S.H., Esser, B., 2016. Multi-tracer approach (^{18}O, ^{3}H/^{3}He, CFC, SF_6, ^{35}S) to find the best emergency drinking water supply, Vorarlberg, Austria. Geophys. Res. Abstr. 18. https://meetingorganizer.copernicus.org/EGU2016/EGU2016-14354.pdf (EGU2016-14354).
Krishnaswami, S., Seidemann, D.E., 1988. Comparative study of ^{222}Rn, ^{40}Ar, ^{39}Ar and ^{37}Ar leakage from rocks and minerals: implications for the role of nanopores in gas transport through natural silicates. Geochim. Cosmochim. Acta 52, 655–658. https://doi.org/10.1016/0016-7037(88)90327-4.
Krishnaswamie, S., Graustein, C., Turekian, K.K., Dowd, J., 1982. Radium, thorium and radioactive lead isotopes in groundwaters: application to the in situ determination of adsorption-desorption rate constants and retardation factors. Water Resour. Res. 18 (6), 1633–1675.
Kurita, N., Hirasawa, N., Motoyama, H., Nakazawa, F., Akata, N., Poluianov, S., 2019. Recent spatial distribution of tritium concentration in surface snow over East Antarctica. In: Proceedings of the 10th Symposium on Polar Science. Glaciology, Session Polar Meteorology and. https://nipr.repo.nii.ac.jp/records/15790.
Kusmierczyk-Michulec, J., Gheddou, A., Nikkinen, M.T., 2015. Influence of precipitation on ^{7}Be concentrations in air as measured by CTBTO global monitoring system. J. Environ. Radioact. 144, 140–151.
Ladouche, B., Probst, A., Viville, D., Idir, S., Baqué, D., Loubet, M., et al., 2001. Hydrograph separation using isotopic, chemical and hydrological approaches (Strengbach catchment, France). J. Hydrol. 242 (3–4), 255–274.
Lal, D., Lee, T., 1988. Cosmogenic ^{32}P and ^{33}P used as tracers to study phosphorus recycling in the ocean. Nature 333, 752–754.
Lal, D., Peters, B., 1967. Cosmic ray produced radioactivity on the Earth. In: Sittle, K. (Ed.), Handbuch der Physik/Encyclopedia of Physics. Springer, Berlin, Heidelberg, Germany, pp. 551–612. https://doi.org/10.1007/978-3-642-46079-1_7.
Lal, D., Narasappaya, N., Zutshi, P.K., 1957. Phosphorus isotopes ^{32}P and ^{33}P in rain water. Nucl. Phys. 3, 69–75.
Lane-Smith, D., Schubert, M., 2020. Absolute measurement of thoron in surface waters. Water 12, 3083. https://doi.org/10.3390/w12113083.
Lange, C., 1994. Size distribution of atmospheric particles containing beryllium-7. J. Aerosol Sci. 25, 45–46.
Lapp, A., 2015. Seasonal Variability of Groundwater Contribution to Watershed Discharge in Discontinuous Permafrost in the North Klondike River Valley, Yukon (Doctoral dissertation). Université d'Ottawa/University of Ottawa.
László, E., Palcsu, L., Leelőssy, Á., 2020. Estimation of the solar-induced natural variability of the tritium concentration of precipitation in the northern and southern Hemisphere. Atmos. Environ. 233, 117605.
Liao, F., Wang, G., Shi, Z., Cheng, G., Kong, Q., Mu, W., Guo, L., 2018. Estimation of groundwater discharge and associated chemical fluxes into Poyang Lake, China: approaches using stable isotopes (δD and δ18 O) and radon. Hydrogeol. J. 26 (5), 1625–1638. https://doi.org/10.1007/s10040-018-1793-3.
Liao, F., Cardenas, M.B., Ferencz, S.B., Chen, X., Wang, G., 2021. Tracing bank storage and hyporheic exchange dynamics using ^{222}Rn: virtual and field tests and comparison with other tracers. Water Resour. Res. 57 (5), e2020WR028960.
Lin, M., Thiemens, M.H., 2018. Accurate quantification of radiosulfur in chemically complex atmospheric samples. Anal. Chem. 90, 2884–2890.
Lin, M., Thiemens, M.H., 2022. Cosmogenic radiosulfur tracking of solar activity and the strong and long-lasting El Nino events. Proc. Natl. Acad. Sci. U. S. A. 119 (19), e2121550119.
Lin, Y.C., Huh, C.A., Hsu, S.C., Lin, C.Y., Liang, M.C., Lin, P.H., 2014. Stratospheric influence on the concentration and seasonal cycle of lower tropospheric ozone: observation at Mount Hehuan. Taiwan. Geophys. Res. Atmos. 119 (6), 3527–3536.
Lin, M., Su, L., Shaheen, R., Fung, J.C.H., Thiemens, M.H., 2016. Detection of deep stratospheric intrusions by cosmogenic ^{35}S. Proc. Natl. Acad. Sci. U. S. A. 113 (40), 11131–11136.
Lin, M., Wang, K., Kang, S., Thiemens, M.H., 2017. Simple method for high-sensitivity determination of cosmogenic ^{35}S in snow and water samples collected from remote regions. Anal. Chem. 89, 4116–4123.
Lin, M., Wang, K., Kang, S., Li, Y., Fan, Z., Thiemens, M.H., 2021. Isotopic signatures of stratospheric air at the Himalayas and beyond. Sci. Bull. 66, 323–326.
Lindsey, B.D., Jurgens, B.C., Belitz, K., 2019. Tritium as an indicator of modern, mixed, and premodern groundwater age. Scientific Investigations Report-US Geological Survey 5090. https://doi.org/10.3133/sir20195090.
Loosli, H.H., Oeschger, H., 1979. Argon-39, Carbon-14 and Krypton-85 measurements in groundwater samples. In: International Symposium on Isotope Hydrology–Proceedings. IAEA, Vienna, pp. 931–947.
Lovley, D.R., Chapelle, F.H., 1995. Deep subsurface microbial processes. Rev. Geophys. 33, 365–381.
Luek, J.L., Beck, A.J., 2014. Radium budget of the York River estuary (VA, USA) dominated by submarine groundwater discharge with a seasonally variable groundwater end-member. Mar. Chem. 165, 55–65.
Ma, Q., Zhang, Y., 2020. Global research trends and hotspots on submarine groundwater discharge (SGD): a bibliometric analysis. Int. J. Environ. Res. Public Health 17 (3), 830, 2020.
MacIntyre, S., 1995. Trace gas exchange across the air-sea interface in fresh water and coastal marine environments. In: Biogenic Trace Gases: Measuring Emissions from Soil and Water. Blackwell Science, pp. 52–97.
Masarik, J., Beer, J., 1999. Simulation of particle fluxes and cosmogenic nuclides production in the earth's atmosphere. J. Geophys. Res. 104, 12099–12112.
Matsumoto, T., Maruoka, T., Shimoda, G., Obata, H., Kagi, H., Suzuki, K., et al., 2013. Tritium in Japanese precipitation following the March 2011 Fukushima Daiichi nuclear plant accident. Sci. Total Environ. 445, 365–370.
Mayo, A., Tingey, D., 2022. Continental Interior Storm Tracks, Tritium Deposition, and Precipitation Isotopes at the Great Basin-Rocky Mountain Physiographic Provinces Transition Zone. Earth Space Sci Open Archive, USA. https://doi.org/10.1002/essoar.10506861.1.
McMahon, T.A., Denison, P.J., 1979. Empirical atmospheric deposition parameters – a survey. Atmos. Environ. 13, 571–585.
McNeary, D., Baskaran, M., 2003. Depositional characteristics of ^{7}Be and ^{210}Pb in southeastern Michigan. J. Geophys. Res. 108 (D7), 4210.
Medici, F., 2001. The IMS radionuclide network of the CTBT. Radiat. Phys. Chem. 161, 689–690.
Mekhaldi, F., Adolphi, F., Herbst, K., Muscheler, R., 2021. The signal of solar storms embedded in cosmogenic radionuclides: detectability and uncertainties. J. Geophys. Res. Space Physics 126 (8), e2021JA029351.
Meredith, E.L., Kuzara, S.L., 2012. Identification and quantification of base flow using carbon isotopes. Groundwater 50, 959–965. https://doi.org/10.1111/j.1745-6584.2012.00952.x.
Michel, R.L., Campbell, D., Clow, D., Turk, J.T., 2000. Timescales for migration of atmospherically derived sulfate through an alpine/subalpine watershed, Loch Vale. Colorado. Water Resour. Res. 36, 27–36.
Michel, R.L., Turk, J.T., Campbell, D., Turk, M.A., 2002. Use of natural ^{35}S to trace sulphate cycling in small lakes, Flattops Wilderness Area, Colorado, U.S.A. Water Air Soil Pollut.: Focus, 2, pp. 5–18.
Mohan, M.P., D'Souza, R.S., Nayak, S.R., Kamath, S.S., Shetty, T., Kumara, K.S., Yashodhara, I., Mayya, Y.S., Karunakara, N., 2018. A study of temporal variations of 7Be and 210Pb concentrations and their correlations with rainfall and other parameters in the South West Coast of India. J. Environ. Radioact. 192, 194–207. https://doi.org/10.1016/j.jenvrad.2018.06.018.
Molina-Porras, A., Condomines, M., Legeay, P.L., Bailly-Comte, V., Seidel, J.L., 2020. Radium Isotopes as a Tracer of Water Sources and Mixing in the Vidourle Stream

(South of France). Aquat. Geochem. 26, 119–136. https://doi.org/10.1007/s10498-020-09371-1.
Montiel, D., Lamore, A.F., Stewart, J., Lambert, W.J., Honeck, J., Lu, Y., et al., 2019. Natural groundwater nutrient fluxes exceed anthropogenic inputs in an ecologically impacted estuary: lessons learned from Mobile Bay, Alabama. Biogeochemistry 145 (1), 1–33. https://doi.org/10.1007/s10533-019-00587-0.
Moore, W.S., 1976. Sampling 228Ra in the deep ocean. Deep-Sea Res. Oceanogr. Abstr. 23 (7), 647–651. https://doi.org/10.1016/0011-7471(76)90007-3.
Moore, W.S., 2000. Determining coastal mixing rates using radium isotopes. Cont. Shelf Res. 20 (15), 1993–2007. https://doi.org/10.1016/S0278-4343(00)00054-6.
Moore, W.S., Arnold, R., 1996. Measurement of ^{223}Ra and ^{224}Ra in coastal waters using a delayed coincidence counter. J. Geophys. Res. 101, 1321–1329.
Moore, W.S., Reid, D.F., 1973. Extraction of radium from natural waters using manganese-impregnated acrylic fibers. J. Geophys. Res. 78, 8880–8886.
Morel, C., Fardeau, J.C., 1989. The uptake by crops of fresh and residual phosphatic fertilizers by simultaneous measurements with ^{32}P and ^{33}P. International Journal of Radiation Applications and Instrumentation. Part A. Appl. Radiat. Isot. 40 (4), 273–278.
Morera-Gómez, Y., Alonso-Hernández, C.M., Cartas-Águila, H.A., 2022. 10-Years assessment of 7Be and 210Pb in atmospheric bulk depositions in Cienfuegos (Cuba). J. Environ. Radioact. 246, 106831 https://doi.org/10.1016/j.jenvrad.2022.106831.
Morgenstern, U., Taylor, C.B., 2009. Ultra low-level tritium measurement using electrolytic enrichment and LSC. Isot. Environ. Health Stud. 45 (2), 96–117.
Nazaroff, W.W., 1992. Radon transport from soil to air. Rev. Geophys. 30 (2), 137–160.
Nazaroff, W.W., Nero Jr., A.V., 1988. Radon and its Decay Products in Indoor Air. John Wiley & Sons, New York/NY/USA.
Novák, M., Přechová, E., 1995. Movement and transformation of ^{35}S-labelled sulphate in the soil of a heavily polluted site in the northern Czech Republic. Environ. Geochem. Health 17, 83–94. https://doi.org/10.1007/BF00146710.
Olid, C., Rodellas, V., Rocher-Ros, G., Garcia-Orellana, J., Diego-Feliu, M., Alorda-Kleinglass, A., Bastviken, D., Karlsson, J., 2022. Groundwater discharge as a driver of methane emissions from Arctic lakes. Nat. Commun. 13, 3667.
Ortega, L., Manzano, M., Custodio, E., Hornero, J., Rodríguez-Arévalo, J., 2015. Using ^{222}Rn to identify and quantify groundwater inflows to the Mundo River (SE Spain). Chem. Geol. 395, 67–79.
Osaki, S., Tagawa, Y., Chijiiwa, T., Sugihara, S., Maeda, Y., 1999. Atmospheric deposition of 35S. J. Radioanal. Nucl. Chem. 239 (3), 543–547. https://doi.org/10.1007/BF02349066.
Palcsu, L., Morgenstern, U., Sültenfuss, J., Koltai, G., László, E., Temovski, M., Major, Z., Nagy, J.T., Papp, L., et al., 2018. Modulation of cosmogenic tritium in meteoric precipitation by the 11-year cycle of solar magnetic field activity. Sci. Rep. 8, 12813 https://doi.org/10.1038/s41598-018-31208-9.
Papastefanou, C., Ioannidou, A., 1995. J. Environ. Radioact. 26, 273–282. https://doi.org/10.1016/0265-931X(94)00011-K.
Penna, D., van Meerveld, H.J., 2019. Spatial variability in the isotopic composition of water in small catchments and its effect on hydrograph separation. Wiley Interdiscip. Rev.: Water 6 (5), e1367.
Petermann, E., Knöller, K., Rocha, C., Scholten, J., Stollberg, R., Weiß, H., Schubert, M., 2018a. Coupling end-member mixing analysis and isotope mass balancing (222-Rn) for differentiation of fresh and re-circulated submarine groundwater discharge (SGD) into Knysna estuary, South Africa. J. Geophys. Res. 123, 1–19. https://doi.org/10.1002/2017JC013008.
Petermann, E., Gibson, J.J., Knöller, K., Pannier, T., Weiß, H., Schubert, M., 2018b. Determination of groundwater discharge rates and water residence time of groundwater-fed lakes by stable isotopes of water (δ^{18}O, δ^{2}H) and radon (^{222}Rn) mass balances. Hydrol. Process. 32 (6), 805–816.
Pham, M.K., Betti, M., Nies, H., Povinec, P.P., 2011. Temporal changes of 7Be, 137Cs and 210Pb activity concentrations in surface air at Monaco and their correlation with meteorological parameters. J. Environ. Radioact. 102 (11), 1045–1054. https://doi.org/10.1016/j.jenvrad.2011.06.002.
Pinay, G., Peiffer, S., De Dreuzy, J.R., Krause, S., Hannah, D.M., Fleckenstein, J.H., et al., 2015. Upscaling nitrogen removal capacity from local hotspots to low stream orders' drainage basins. Ecosystems 18, 1101–1120.
Plummer, L.N., Bexfield, L.M., Anderholm, S.K., Sanford, W.E., Busenberg, E., 2001. Geochemical characterization of ground-water flow in parts of the Santa Fe Group Aquifer System, Middle Rio Grande Basin, New Mexico - U.S. Geological Survey Middle Rio Grande Basin Study. In: COLE, J.C. (Ed.), Proc. 4th Annu. Workshop Albuquerque, NM, 2000, Open File Rep. 00-488. US Geological Survey, Denver, CO, pp. 7–10.
Poluianov, S.V., Kovaltsov, G.A., Mishev, A.L., Usoskin, I.G., 2016. Production of cosmogenic isotopes ^{7}Be, ^{10}Be, ^{14}C, ^{22}Na, and ^{36}Cl in the atmosphere: altitudinal profiles of yield functions. J. Geophys. Res. Atmos. 121, 8125–8136.
Poluianov, S.V., Kovaltsov, G.A., Usoskin, I.G., 2020. A new full 3-D model of cosmogenic tritium ^{3}H production in the atmosphere (CRAC: ^{3}H). J. Geophys. Res. Atmos. 125 (18), e2020JD033147.
Poreda, R.J., Cerling, T.E., Salomon, D.K., 1988. Tritium and helium isotopes as hydrologic tracers in a shallow unconfined aquifer. J. Hydrol. 103 (1–2), 1–9.
Prichard, H.W., Gesell, T.F., 1977. Rapid measurements of 222Rn concentrations in water with a commercial liquid scintillation counter. Health Phys. 33 (6), 577–581. https://doi.org/10.1097/00004032-197712000-00008.
Priebe, E.H., Hamilton, S.M., Lemieux, A., Rowan, D.J., Clark, I.D., 2023. Tritium across the hydrologic systems of southern Ontario, Canada: implications for groundwater age dating in the Great Lakes Basin. Hydrogeol. J. 31 (3), 641–659.
Priyadarshi, A., Dominguez, G., Thiemens, M.H., 2011. Evidence of neutron leakage at the Fukushima nuclear plant from measurements of radioactive ^{35}S in California. Proc. Natl. Acad. Sci. U. S. A. 108 (35), 14422–14425.
Priyadarshi, A., Hill-Falkenthal, J., Thiemens, M.H., Yoshida, N., Toyoda, S., Yamada, K., Mukotaka, A., Fujii, A., Uematsu, M., Hatekeyama, S., Noguchi, I., Nojiri, Y., Tanimoto, H., 2013. Detection of radioactive ^{35}S at Fukushima and other Japanese sites. J. Geophys. Res. Atmos. 118 (2), 1020–1027.
Qiao, J., Colgan, W., Jakobs, G., Nielsen, S., 2021. High-resolution tritium profile in an ice core from camp century. Greenland. Environ. Sci. Technol. 55 (20), 13638–13645.
Rama, Moore, W.S., 1996. Using the radium quartet for evaluating groundwater input and water exchange in salt marshes. Geochim. Cosmochim. Acta 60 (23), 4645–4652. https://doi.org/10.1016/S0016-7037(96)00289-X.
Rank, D., Özsoy, E., Salihoğlu, I., 1999. Oxygen-18, deuterium and tritium in the Black Sea and the Sea of Marmara. J. Environ. Radioact. 43, 231–245.
Raymond, P.A., Zappa, C.J., Butman, D., Bott, T.L., Potter, J., Mulholland, P., Laursen, A. E., McDowell, W.H., Newbold, D., 2012. Scaling the gas transfer velocity and hydraulic geometry in streams and small rivers. Limnol. Oceanogr. Fluids Environ. 2, 41–53.
Raymond, P.A., Saiers, J.E., Sobczak, W.V., 2016. Hydrological and biogeochemical controls on watershed dissolved organic matter transport: pulse-shunt concept. Ecology 97 (1), 5–16.
Rocha, C., Wilson, J., Scholten, J., Schubert, M., 2015. Retention and fate of groundwater-borne Nitrogen in a coastal bay (Kinvarra Bay, Western Ireland) during summer. Biogeochemistry 125, 275–299. https://doi.org/10.1007/s10533-015-0116-1.
Rodellas, V., Garcia-Orellana, J., Trezzi, G., Masqué, P., Stieglitz, T.C., Bokuniewicz, H., Berdalet, E., 2017. Using the radium quartet to quantify submarine groundwater discharge and porewater exchange. Geochim. Cosmochim. Acta 196, 58–73.
Rösler, H.J., 1984. Lehrbuch der Mineralogie. Deutscher Verlag für Grundstoffindustrie, Leipzig/Deutschland.
Sadler, S. 2023. pers. comm.
Savoy, L., Surbeck, H., Hunkeler, D., 2011. Radon and CO_2 as natural tracers to investigate the recharge dynamics of karst aquifers. J. Hydrol. 406 (3–4), 148–157.
Schmidt, A., Schubert, M., 2007. Using ^{222}Rn as environmental tracer for assessing groundwater / surface water interaction. Geochim. Cosmochim. Acta 71 (15S), A894.
Schmidt, A., Schlüter, M., Melles, M., Schubert, M., 2008. Continuous and discrete on-site detection of radon-222 in ground- and surface waters by means of an extraction module. Appl. Radiat. Isot. 66, 1939–1944.
Schmidt, A., Stringer, C.E., Haferkorn, U., Schubert, M., 2009. Quantification of groundwater discharge into lakes using radon-222 as naturally occurring tracer. Environ. Geol. 56, 855–863.
Schmidt, A., Gibson, J.J., Santos, I.R., Schubert, M., Tattrie, K., Weiss, H., 2010. The contribution of groundwater discharge to the overall water budget of two typical Boreal lakes in Alberta/Canada estimated from a radon mass balance. Hydrol. Earth Syst. Sci. 14, 79–89.
Schmidt, A., Frank, G., Stichler, W., Duester, L., Steinkopff, T., Stumpp, C., 2020. Overview of tritium records from precipitation and surface waters in Germany. Hydrol. Process. 34 (6), 1489–1493.
Schubert, M., Bürkin, W., Peña, P., Lopez, A., Balcázar, M., 2006. On-site determination of the radon concentration in water samples: methodical background and results from laboratory studies and a field-scale test. Radiat. Meas. 41, 492–497.
Schubert, M., 2015. Using radon as environmental tracer for the assessment of subsurface Non-Aqueous Phase Liquid (NAPL) contamination - a review. Eur. Phys. J. Special Topics 224, 717–730.
Schubert, M., Paschke, A., Lieberman, E., Burnett, W.C., 2012. Air-water partitioning of 222Rn and its dependence on water salinity. Environ. Sci. Technol. 46, 3905–3911.
Schubert, M., Kopitz, J., Chałupnik, S., 2014. Sample volume optimization for radon-in-water detection by liquid scintillation counting. J. Environ. Radioact. 134, 109–113.
Schubert, M., Knoeller, K., Einsiedl, F., Rocha, C., 2015. Preliminary evaluation of groundwater contributions to the water budget of Kinvarra Bay, Ireland, using ^{222}Rn, EC and stable isotopes as natural indicators. Environ. Monit. Assess. 187 (3), 4274. https://doi.org/10.1007/s10661-015-4274-3.
Schubert, M., Knöller, K., Stollberg, R., Mallast, U., Ruzsa, G., Melikadze, G., 2017. Evidence for submarine groundwater discharge into the Black Sea – investigation of two dissimilar geographical settings. Water 9 (7), 468–480. https://doi.org/10.3390/w9070468.
Schubert, M., Kopitz, J., Knöller, K., 2019. Improved approach for LSC detection of ^{35}S aiming at its application as tracer for short groundwater residence times. J. Environ. Radioact. 208-209, 106022 https://doi.org/10.1016/j.jenvrad.2019.106022.
Schubert, M., Knöllner, K., Tegen, I., Terzi, L., 2020a. Variability of cosmogenic ^{35}S in rain-resulting implication for the use of radiosulfur as natural groundwater residence time tracer. Water 12. https://doi.org/10.3390/w1210299953.
Schubert, M., Siebert, C., Knoeller, K., Roediger, T., Schmidt, A., Gilfedder, B., 2020b. Investigating groundwater discharge into a major river under low flow conditions based on a radon mass balance supported by tritium data. Water 12. https://doi.org/10.3390/w12102838.
Schubert, M., Knöller, K., Müller, Ch., Gilfedder, B., 2020c. Investigating river water/groundwater interaction along a rivulet section by ^{222}Rn mass balancing. Water 12. https://doi.org/10.3390/w12113027.
Schubert, M., Kopitz, J., Knöller, K., 2020d. Low-sulphate water sample preparation for LSC detection of ^{35}S avoiding sulphate precipitation. J. Environ. Radioact. 213, 106153 https://doi.org/10.1016/j.jenvrad.2019.106153.
Schubert, M., Weise, S.M., Knöller, K., 2021. Atmospheric washout of ^{35}S during single rain events – implications for ^{35}S sampling schemes. J. Environ. Radioact. 237, 106669.
Schubert, M., Scholten, J., Kreuzburg, M., Petermann, E., Lopes de Paiva, M., Köhler, D., Liebetrau, V., Rapaglia, J., Schlüter, M., 2022. Radon (^{222}Rn) as tracer for submarine

groundwater discharge investigation – limitations of the approach at shallow wind-exposed coastal settings. Environ. Monit. Assess. 194, 798. https://doi.org/10.1007/s10661-022-10462-5.
Schubert, M., Knoeller, K., Scholten, J., Reyes Bravo, M.M., Chávez Solís, E.M., Daesslé, L.W., 2023. Quantification of groundwater discharge into a shallow coastal lagoon applying a multi-tracer approach. Environ. Monit. Assess. 195 (601) https://doi.org/10.1007/s10661-023-11244-3.
Schubert, M., Bollhöfer, A., Schmidt, A., 2024. Radiosulphur as Water Residence Time Tracer – Straightforward Approach for Setting Up a ^{35}S Input Function Based on ^{3}H and ^{7}Be Datasets (In prep).
Schulze, J., Auer, M., Werzi, R., 2000. Low level radioactivity measurement in support of the CTBTO. Appl. Radiat. Isot. 53, 23–30.
Schumann, R.R., Gundersen, L.C.S., 1996. Geologic and climatic controls on the radon emanation coefficient. Environ. Int. 22 (1), 439–446.
Schürch, M., Kozel, R., Schotterer, U., Tripet, J.P., 2003. Observation of isotopes in the water cycle - the Swiss National Network (NISOT). Environ. Geol. 45, 1–11.
Silker, W.B., Perkins, R.W., Rieck, H.G., 1971. A sampler for concentrating radionuclides from natural waters. Ocean Eng. 2 (2), 49–55.
Skerlak, B., Sprenger, M., Wernli, H., 2014. A global climatology of stratosphere-troposphere exchange using the ERA-Interim data set from 1979 to 2011. Atmos. Chem. Phys. 14, 913–917.
Smith, J.T., Bowes, M.J., Cailes, C.R., 2011. A review and model assessment of ^{32}P and ^{33}P uptake to biota in freshwater systems. J. Environ. Radioact. 102 (4), 317–325.
Snow, D.D., Spalding, R.F., 1997. Short-term aquifer residence times estimated from ^{222}Rn disequilibrium in artificially-recharged ground water. J. Environ. Radioact. 37 (3), 307–325.
Somaratne, N., Zulfic, H., Ashman, G., Vial, H., Swaffer, B., Frizenschaf, J., 2013. Groundwater risk assessment model (GRAM): groundwater risk assessment model for wellfield protection. Water 5 (3), 1419–1439. https://doi.org/10.3390/w5031419.
Sprenger, C., Lorenzen, G., Hülshoff, I., Grützmacher, G., Ronghang, M., Pekdeger, A., 2011. Vulnerability of bank filtration systems to climate change. Sci. Total Environ. 409, 655–663. https://doi.org/10.1016/j.scitotenv.2010.11.002.
Stewart, M.K., Morgenstern, U., McDonnell, J.J., 2010. Truncation of stream residence time: how the use of stable isotopes has skewed our concept of stream water age and origin. Hydrol. Process. 24 (12), 1646–1659.
Strong, K.P., Lewins, D.M., 1982. Effect of moisture content on radon emanation from uranium ore and tailings. Health Phys. 42 (1), 27–32.
Sturchio, N.C., Du, X., Purtschert, R., Lehmann, B.E., Sultan, M., Patterson, L.J., et al., 2004. One million year old groundwater in the Sahara revealed by krypton-81 and chlorine-36. Geophys. Res. Lett. 31, L05503 https://doi.org/10.1029/2003GL019234.
Suckow, A., 2014. The age of groundwater – definitions, models and why we do not need this term. J. Appl. Geochem. 50, 222–230.
Sukanya, S., Noble, J., Joseph, S., 2022. Application of radon (^{222}Rn) as an environmental tracer in hydrogeological and geological investigations: an overview. Chemosphere 303 (3), 135141.
Tadros, C.V., Hughes, C.E., Crawford, J., Hollins, S.E., Chisari, R., 2014. Tritium in Australian precipitation: a 50 year record. J. Hydrol. 513, 262–273.
Tanaka, N., Turekian, K.K., 1991. Use of cosmogenic ^{35}S to determine the rates of removal of atmospheric SO_2. Nature 352, 226–228.
Taylor, A., Keith-Roach, M.J., Iurian, A.R., Mabit, L., Blake, W.H., 2016. Temporal variability of beryllium-7 fallout in southwest UK. J. Environ. Radioact. 160, 80–86. https://doi.org/10.1016/j.jenvrad.2016.04.025. https://www.sciencedirect.com/science/article/pii/S0265931X16301230.
Taylor, A., Blake, W.H., Iurian, A.R., Millward, G.E., Mabit, L., 2019. The use of Be-7 as a soil and sediment tracer. In: Mabit, L., Blake, W.H. (Eds.), Assessing Recent Soil Erosion Rates Through the Use of Beryllium-7 (Be-7). Springer, pp. 1–13.
Terzer-Wassmuth, S., Araguas-Araguas, L.J., Copia, L., Miller, J.A., 2022a. Space or climate? Disentangling cosmogenic and climatic drivers of present-day tritium (^{3}H) in global precipitation. In: EGU General Assembly Conference Abstracts pp. EGU22-11230.
Terzer-Wassmuth, S., Araguás-Araguás, L.J., Copia, L., Wassenaar, L.I., 2022b. High spatial resolution prediction of tritium (^{3}H) in contemporary global precipitation. Sci. Rep. 12 (1), 10271.
Terzi, L., Kalinowski, M., 2017. World-wide seasonal variation of ^{7}Be related to large-scale atmospheric circulation dynamics. J. Environ. Radioact. 178-179, 1–15.
Terzi, L., Kalinowski, M., Schoeppner, M., Wotawa, G., 2019. How to predict seasonal weather and monsoons with radionuclide monitoring. Sci. Rep. Nature Research 9, 2729. https://doi.org/10.1038/s41598-019-39664-7.
Terzi, L., Wotawa, G., Schoeppner, M., et al., 2020. Radioisotopes demonstrate changes in global atmospheric circulation possibly caused by global warming. Sci. Rep. Nature Research 10, 10695. https://doi.org/10.1038/s41598-020-66541-5.
Tilley, D.R., Cheves, C., Godwin, J., Hale, G., Hofmann, H., Kelley, J., Sheu, C., Weller, H., 2002. Energy levels of light nuclei A = 5, 6, 7. Nucl. Phys. A 708, 3–163.
Turekian, K.K., Tanaka, N., 1992. The use of atmospheric cosmogenic ^{35}S and ^{7}Be in determining depositional fluxes of SO_2. Geophys. Res. Lett. 19 (17), 1767–1770.
Unland, N.P., Cartwright, I., Andersen, M.S., Rau, G.C., Reed, J., Gilfedder, B.S., Atkinson, A.P., Hofmann, H., 2013. Investigating the spatio-temporal variability in groundwater and surface water interactions: a multi-technical approach. Hydrol. Earth Syst. Sci. 17 (9), 3437–3453.
Uriostegui, S.H., Bibby, R.K., Esser, B.K., Clark, J.F., 2015. Analytical method for measuring cosmogenic ^{35}S in natural waters. Anal. Chem. 87, 6064–6070.
Uriostegui, S.H., Bibby, R.K., Esser, B.K., Clark, J.F., 2016. Quantifying groundwater travel time near managed aquifer recharge operations using ^{35}S as an intrinsic tracer. J. Hydrol. https://doi.org/10.1016/j.hydrol.2016.04.036.
Uriostegui, S.H., Bibby, R.K., Esser, B.K., Clark, J.F., 2017. Quantifying annual groundwater recharge and storage in the Central Sierra Nevada using naturally-occurring ^{35}S. Hydrol. Process. 31, 1382–1397. https://doi.org/10.1002/hyp.11112.
Usoskin, I.G., Kovaltsov, G.A., 2008. Production of cosmogenic Be7 isotope in the atmosphere: full 3-D modeling. J. Geophys. Res. 113, D12107 https://doi.org/10.1029/2007JD009725.
Vallés, I., Camacho, A., Ortega, X., Serrano, I., Blázquez, S., Pérez, S., 2009. Natural and anthropogenic radionuclides in airborne particulate samples collected in Barcelona (Spain). J. Environ. Radioact. 100 (2), 102–107. https://doi.org/10.1016/j.jenvrad.2008.10.009.
Van der Velde, Y., de Rooij, G.H., Rozemeijer, J.C., van Geer, F.C., Broers, H.P., 2010. Nitrate response of a lowland catchment: on the relation between stream concentration and travel time distribution dynamics. Water Resour. Res. 46, W11534 https://doi.org/10.1029/2010WR009105.
Varlam, C., Patrascu, V., Margineanu, R.M., Faurescu, I., Vagner, I., Faurescu, D., Duliu, O.G., 2013. Tritium activity concentration along the Western shore of the Black Sea. J. Radioanal. Nucl. Chem. 298, 1679–1683.
Vautier, C., Abhervé, R., Chatton, E., Labasque, T. de Dreuzy, J.R., 2020. A new method to quantify air-water gas exchanges in streams based on slug injection and semicontinuous measurement. Limnol. Oceanogr. Methods 18, 453–465. doi:https://doi.org/10.1002/lom3.10376.
Veselý, J., Beneš, P., Ševčí, K., 1989. Occurrence and speciation of beryllium in acidified freshwaters. Water Res. 23 (6), 711–717.
Visser, A., Thaw, M., Deinhart, A., Bibby, R., Safeeq, M., Conklin, M., Esser, B., Van der Velde, Y., 2019. Cosmogenic isotopes unravel the hydrochronology and water storage dynamics of the southern sierra critical zone. Water Resour. Res. 55 (2), 1429–1450. https://doi.org/10.1029/2018WR023665.
Vogel, J.C., Thilo, L., van Dijken, M., 1974. Determination of groundwater recharge with tritium. J. Hydrol. 23 (1–2), 131–140.
von Freyberg, J., Studer, B., Rinderer, M., Kirchner, J.W., 2018. Studying catchment storm response using event- and pre-event-water volumes as fractions of precipitation rather than discharge. Hydrol. Earth Syst. Sci. 22, 5847–5865. https://doi.org/10.5194/hess-22-5847-2018.
Wang, H., Knabe, D., Engelhardt, I., Droste, B., Rohns, H.P., Stumpp, C., et al., 2022. Dynamics of pathogens and faecal indicators during riverbank filtration in times of high and low river levels. Water Res. 209, 117961.
Wang, D., Chadwick, D.R., Hill, P.W., Ge, T., Jones, D.L., 2023. Tracing the mineralization rates of C, N and S from cysteine and methionine in a grassland soil: a ^{14}C and ^{35}S dual-labelling study. Soil Biol. Biochem. 177 https://doi.org/10.1016/j.soilbio.2022.108906.
Warr, O., Smith, N.J.T., Sherwood Lollar, B., 2023. Hydrogeochronology: resetting the timestamp for subsurface groundwaters. Geochim. Cosmochim. Acta 348, 221–238.
Waser, N.A.D., Bacon, M.P., 1995. Wet deposition fluxes of cosmogenic ^{32}P and ^{33}P the $^{33}P/^{32}P$ ratios at Bermuda. Earth Planet. Sci. Lett. 133, 71–80.
Waser, N.A.D., Fleer, A.F., Hammar, T.R., Buesseler, K.O., Bacon, M.P., 1994. Determination of natural ^{32}P and ^{33}P in rainwater, marine particles and plankton by low-level beta counting. Nucl. Instrum. Meth. Phys. A338, 560–567.
Webb, J.R., Santos, I.R., Robson, B., Macdonald, B., Jeffrey, L., Maher, D.T., 2017. Constraining the annual groundwater contribution to the water balance of an agricultural floodplain using radon: the importance of floods. Water Resour. Res. 53, 544–562. https://doi.org/10.1002/2016WR019735.
Wei, M., 1998. Evaluating AVI and DRASTIC for Assessing Pollution Potential in the Lower Fraser Valley, British Columbia: Aquifer Vulnerability and Nitrate Occurrence. Report, British Columbia, Ministry of Environment, Lands and Parks, Water Management Branch.
Weigel, F., 1978. Radon. Chemiker-Zeitung 102 (9), 287–299.
Welsh, K., Sánchez-Murillo, R., 2020. Rainfall, groundwater, and surface water isotope data from extreme tropical cyclones (2016-2019) within the Caribbean Sea and Atlantic Ocean basins. Data Brief 30, 105633. https://doi.org/10.1016/j.dib.2020.105633.
Wilkening, M., 1974. Radon from the island of Hawaii: deep soils are more important than lava fields or volcanoes. Science 183, 413–415.
Wilkening, M., 1990. Radon in the Environment - Studies in Environmental Science, 40. Elsevier, Amsterdam/Netherlands.
Winkler, R., Dietl, F., Frank, G., Tschiersch, J., 1998. Temporal variation of ^{7}Be and ^{210}Pb size distributions in ambient aerosol. Atmos. Environ. 32, 983–991. https://doi.org/10.1016/S1352-2310(97)00333-6.
Wollenberg, H.A., 1984. Naturally Occurring Radioelements and Terrestrial Gamma-Ray Exposure Rates: An Assessment Based on Recent Geochemical Data. Lawrence Berkley Laboratory Report LBL-18714, Berkley/CA/USA.
Yoon, Y.Y., Ko, K.S., Lee, J.M., 2023. Tritium and ^{35}S activity variation in precipitation in Korea and its application to groundwater age determination. J. Radioanal. Nucl. Chem. 332 (6), 1917–1921.
Zhang, F., Wang, J., Baskaran, M., Zhong, Q., Wang, Y., Paatero, J., Du, J., 2021. A global dataset of atmospheric ^{7}Be and ^{210}Pb measurements: annual air concentration and depositional flux. Earth Syst. Sci. Data 13, 2963–2994. https://doi.org/10.5194/essd-13-2963-2021.
Zheng, M., Sjolte, J., Adolphi, F., Aldahan, A., Possnert, G., Wu, M., Muscheler, R., 2021. Solar and meteorological influences on seasonal atmospheric ^{7}Be in Europe for 1975-2018. Chemosphere 263, 128318.